## MIHC: Multi-View Interpretable Hypergraph Neural Networks with Information Bottleneck for Chip Congestion Prediction

Zeyue Zhang $^{a^*}$  Heng Ping $^{b^*}$  Peiyu Zhang $^b$  Nikos Kanakaris $^c$  Xiaoling Lu $^a$  Paul Bogdan $^{b\dagger}$  Xiongye Xiao $^{d\dagger}$ 

<sup>a</sup>Center for Applied Statistics, School of Statistics, Innovation Platform, Renmin University of China;
 <sup>b</sup>Ming Hsieh Department of Electrical and Computer Engineering, University of Southern California;
 <sup>c</sup>Amazon Web Services, Seattle; and <sup>d</sup>Min H. Kao Department of Electrical Engineering and Computer Science, University of Tennessee, Knoxville

## **Abstract**

With the advancement of artificial intelligence (AI) and increasing integrated circuit (IC) design complexity, efficient chip design through electronic design automation (EDA) has become critical. Fast and accurate congestion prediction in chip layout and routing can significantly enhance automated design performance. Existing congestion modeling methods are limited by (i) ineffective processing and fusion of multi-view circuit data information, and (ii) insufficient reliability and interpretability in the prediction process. To address these challenges, we propose the Multi-view Interpretable Hypergraph for Chip (MIHC), a trustworthy multi-view hypergraph neural network framework that (i) processes both graph and image information in unified hypergraph representations, capturing topological and geometric circuit data; (ii) implements a novel subgraph Information Bottleneck mechanism, identifying critical congestion-correlated regions to guide predictions. This work is the first attempt to incorporate such interpretability into congestion prediction through informative graph reasoning. Experiments show that the MIHC method reduces NMAE by 16.67% and 8.57% in cell-based and grid-based predictions on ISPD2015, and 5.26% and 2.44% on CircuitNet-N28, respectively, compared to state-of-the-art methods. Rigorous cross-design generalization experiments further validate our method's capability to handle entirely unseen circuit designs.

## 1 Introduction

Advances in artificial intelligence (AI) and cyber-physical systems (CPS) [23] require a continuous and increasing demand for computational power supported by integrated circuits (ICs). This necessitates rapid, accurate IC design through electronic design automation (EDA)[12]. Efficient quality assessment of generated circuits is crucial to the design process [9], with circuit congestion prediction being particularly vital as it directly impacts reliability, performance, and manufacturability.

Circuit congestion occurs when routing resources are exceeded by wires attempting to traverse the same physical region [4]. This issue arises when cells (i.e., electronic components) that are logically connected by nets (i.e., connecting wires) are physically placed far apart or when many nets must share limited routing space. These situations commonly result from the mismatch between circuit connectivity requirements and physical layout constraints [10]. Therefore, accurate congestion prediction requires comprehensive analysis of both the logical relationships between cells and nets and their geometric distribution in the physical layout [4, 20, 27].

<sup>\*</sup>Equal contribution.

<sup>&</sup>lt;sup>†</sup>Corresponding authors: pbogdan@usc.edu and xxiao9@utk.edu.

Given this dual nature of congestion formation, circuit congestion prediction primarily involves two types of data: *netlist* and *layout*. *Netlist* captures logical connections between cells and nets, representing topological information naturally modeled as graphs. *Layout* data divides the placement area into grids containing circuit features like cell and net density, encoding geometric information in an image-like format. Effective congestion prediction requires processing and fusion of both complementary information types, as congestion patterns are determined by both connection topology and component geometric distribution.

Traditional congestion prediction approaches use rule-based systems [18] and statistical models [16], but struggle with modern circuit complexity [15]. Deep learning (DL) methods have emerged with superior performance, divided into single-view and multi-view approaches. Single-view methods include DE-HNN [14], which transforms circuit connections into hypergraphs using HGNNs [7] to capture topological information, and GAN-based approaches [26] that process grid-based features as images. However, these single-view approaches inevitably miss valuable information from the complementary perspective.

In an attempt to process both views simultaneously, CircuitGNN [24] incorporates layout information into netlist-based hypergraphs by adding position-aware edges, while Lay-Net[28] introduces specialized HGNN modules into Swin-Transformer-based layout processing. However, these methods tend to favor one view while incorporating the other as supplementary information, leading to insufficient fusion of topological and geometric information. Moreover, existing deep learning approaches operate as black boxes, lacking interpretability and trustworthiness crucial for circuit design validation[9, 12].

To address these limitations, we propose the Multi-view Interpretable Hypergraph for Chip (MIHC) framework, a trustworthy multi-view hypergraph neural network-based model featuring symmetrical architecture that fuses netlist and layout data through net-based bridging. Specifically, we construct cell-based and grid-based hypergraphs from respective data sources, with hyperedges in both hypergraphs built through nets, enabling balanced fusion of topological and geometric information. Furthermore, we incorporate a novel subgraph information bottleneck (IB) [17] mechanism that identifies critical congestion-correlated regions, guiding focused prediction while revealing areas needing optimization. This mechanism enhances accuracy through targeted information processing while providing interpretability by revealing the critical local structures causing congestions in circuit design. Such insights are particularly important since congestion typically emerges from interactions between neighboring components rather than isolated elements, offering designers actionable guidance for targeted optimization.

Contributions. The main contributions of this paper are summarized as follows: (1) Multi-View Representation Learning: We propose a novel balanced multi-view HGNN that effectively fuses netlist and layout information through net-based bridging, enabling comprehensive learning of both topological and geometric features for congestion prediction. (2) Interpretable Bottleneck Subgraph: We develop a subgraph IB mechanism that identifies critical regions highly related to congestion, providing interpretability for circuit optimization while improving prediction accuracy through focused learning. (3) Superior Prediction Performance: Comprehensive experiments on the ISPD2015 and CircuitNet-N28 datasets, including rigorous cross-design generalization evaluations, demonstrate that our model reduces NMAE by 16.67% and 8.57% in cell-based and grid-based predictions on ISPD2015, and 5.26% and 2.44% on CircuitNet-N28, respectively, compared to state-of-the-art methods. The evaluation results verify the effectiveness of our multi-view learning strategy and interpretable bottleneck mechanism.

## 2 Related Work

#### 2.1 Deep Learning for Congestion Prediction

Circuit congestion prediction involves processing two types of data: netlist data that can be naturally modeled as graphs, and layout data that can be represented in an image format. Based on how these data types are processed, existing DL approaches can be categorized into single-view and multi-view methods.

**Single-View Methods.** These approaches focus on processing either netlist or layout data exclusively. For netlist-based methods, CongestionNet[9] and Cross-Graph[5] model the netlists as homogeneous graphs and employ GNNs for congestion prediction, while DE-HNN[14] leverages HGNNs to capture

high-order relationships in circuit netlists. For layout-based methods, RouteNet[22] treats grid-based layout data as images and utilizes CNNs to generate congestion maps; CircuitFormer[29] regards the grids of a layout as a point cloud and uses Point Transformer to process each grid. However, these single-view approaches inevitably miss valuable information from the other perspective.

Multi-View Methods. Recent efforts attempt to incorporate both the netlist and layout information. Netlist-centric approaches like the CircuitGNN[24], LHNN[20], and HybridNet[27] construct hypergraphs from netlists and incorporate layout information through position-aware edges or nodes. Layout-centric methods such as Lay-Net[28], DFM-Net[6], and PGNN[1] primarily process grid-based layout data using vision models like U-Net while integrating the netlist information through specialized GNN or HGNN modules. However, these methods tend to favor one data type, often leading to suboptimal and insufficient fusion of topological and geometric information. In contrast, our proposed MIHC model processes both data types by constructing cell-based and grid-based hypergraphs, achieving balanced fusion through net-based bridging.

## 2.2 Interpretation Methods For Graph

In chip congestion prediction, interpretability has received little attention despite being crucial for identifying key performance-enhancing components and transforming black-box approaches into semi-transparent ones that users find more accessible. Since chip congestion prediction naturally involves graph-structured data with complex interactions, we examine graph domain interpretability methods. Existing approaches are primarily post-hoc, such as GNNExplainer [25] and PGExplainer [13], which provide node/edge-level explanations through learned masks but rely on post-hoc strategies for supervised tasks. Recent progress includes self-interpretable methods like SIGNET [11], which generates inherent interpretations during graph anomaly detection. Inspired by these approaches, our MIHC integrates Information Bottleneck [17] to achieve interpretability in chip congestion prediction—representing, to our knowledge, the first interpretability work in this domain.

#### 3 Preliminaries

## 3.1 Problem Formulation

The circuit congestion prediction task aims to estimate the potential congestion levels in a complex circuit design based on its layout and netlist information during early design stages. Congestion can be quantified as the ratio of overflow demand to available routing tracks in IC backend design [3], where overflow represents excess routing requirements beyond provided resources.

Formally, each circuit data is represented as multi-view data comprising grid-based and cell-based information. The grid-based view models circuit layout as a structured grid  $P \in \mathbb{R}^{M \times N \times K}$ , where  $M, N \in \mathbb{N}^+$  are grid dimensions and  $K \in \mathbb{N}^+$  is the number of features per grid cell. The cell-based view represents the circuit at a finer granularity level based on the netlist information, where each cell corresponds to an individual circuit component with specific features. The cell-based view represents the circuit netlist as a hypergraph G = (V, E), where V is the set of nodes (cells) and E is the set of hyperedges (nets connecting multiple cells). Given grid-based representation P and cell-based hypergraph G, our goal is to simultaneously predict a grid congestion map  $C^G \in \mathbb{R}^{M \times N}$  and a cell congestion graph  $C^C \in \mathbb{R}^{|V|}$ , where  $C^G[i,j] \in \mathbb{R}^+$  and  $C^C[k] \in \mathbb{R}^+$  quantify congestion levels at grid (i,j) and cell k, respectively. The notations used in the manuscript are presented in Appendix B.

The predictive model f, parameterized by  $\theta$ , is defined as follows:

$$f_{\theta}: (P,G) \mapsto (\hat{C}^G, \hat{C}^C)$$
 (1)

with the supervised objective to minimize the mean squared error:

$$\mathcal{L}_{\text{sup}} = \frac{1}{M \times N} \sum_{i=1}^{M} \sum_{j=1}^{N} |C^{G}[i,j] - \hat{C}^{G}[i,j]|^{2} + \frac{1}{|V|} \sum_{k=1}^{|V|} |C^{C}[k] - \hat{C}^{C}[k]|^{2}$$
 (2)

## 3.2 Information Bottleneck

The Information Bottleneck (IB) formalism [17] addresses a fundamental challenge in representation learning by extracting the minimal yet sufficient features from high-dimensional data. For example, it

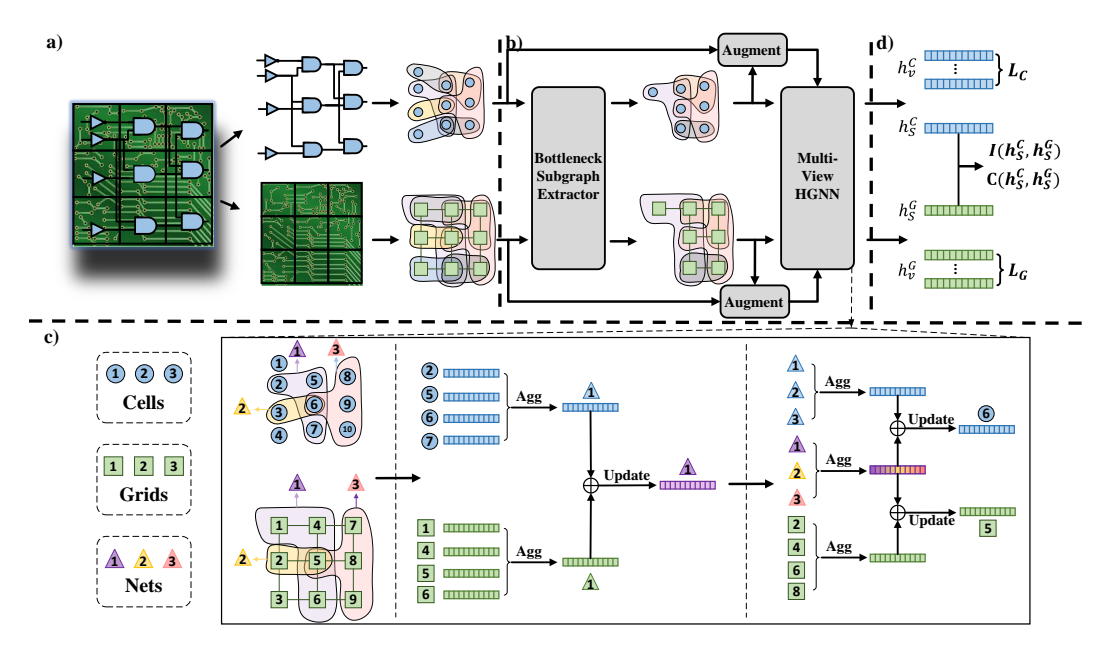


Figure 1: Overview of MIHC framework. (a) Process Module converts raw multi-view data (cell-based netlist and grid-based layout) into hypergraphs  $H^C$  and  $H^G$  (details in Appendix C.2). (b) Interpretable Subgraph Module applies Multi-View Information Bottleneck to extract congestion-correlated bottleneck subgraphs  $H^C_S$  and  $H^G_S$ . (c) Multi-View Representation Learning Module employs MV-HGNN to capture topological and geometric information, generating node embeddings  $h^C_v$ ,  $h^G_v$  and subgraph embeddings  $h^G_S$ ,  $h^G_S$ . (d) Prediction Module uses MLPs to map embeddings to congestion predictions, optimized through supervised, IB, and contrastive losses.

inspired new hierarchical perception methods for multimodal learning [21]. Given an input variable X and target variable Y, IB seeks an intermediate representation T that optimally balances data compression and target information preservation, formulated as:

$$\mathcal{L}[p(t|x)] = I(T;X) - \beta^* I(T;Y),\tag{3}$$

where I(T;X) and I(T;Y) denote mutual information, and  $\beta^* \in \mathbb{R}^+$  controls the compression-relevance trade-off. This formulation enables the identification of critical features driving model predictions while minimizing redundancy, making IB particularly valuable for model interpretability and subgraph analysis in networks [11].

## 4 Method

In this section, we introduce the proposed MIHC framework (see Figure 1) which consists of four parts: (a) The *Process Module* converts raw multi-view data, including cell-based netlist graph and grid-based layout image, into hypergraphs for further processing. (b) The *Interpretable Subgraph Module* introduces a novel subgraph Information Bottleneck (IB) mechanism to identify critical bottleneck subgraphs highly related to circuit congestion and guide the model to focus on these regions during prediction. (c) The *Multi-View Representation Learning Module* integrates both graph and image data into unified hypergraph representations, capturing topological and geometric features of circuit data. (d) The *Prediction Module* computes the prediction in both cell and grid views.

## 4.1 Process Module

Given the dual nature of the data, the Process Module converts raw multi-view data, including both cell-based netlist graph and grid-based layout image, into hypergraphs for subsequent processing.

**Hypergraph Construction from Cell-based Netlist Graph.** We construct a cell-based hypergraph  $H^C = (V^C, E^C)$ , where  $V^C$  represents circuit cells and  $E^C$  represents hyperedges based on net

connections. Each node  $v^C \in V^C$  is initialized with feature  $X_v^C$  derived from circuit netlist characteristics. This hypergraph primarily captures topological relationships among circuit components.

**Hypergraph Construction from Grid-based Layout Image.** We construct a grid-based hypergraph  $H^G = (V^G, E^G)$ , where  $V^G$  represents local layout image regions with feature representation  $X_v^G$  containing each region's component density, and  $E^G$  represents hyperedges connecting these regions. The formation of grid-based hyperedges  $e^G \in E^G$  is guided by spatial proximity and net connections. Hyperedges are established among nodes corresponding to spatially adjacent regions to preserve the geometric information. More importantly, nodes within the same net are grouped into hyperedges to capture high-order geometric information. Both cell-based hyperedges  $E^G$  and grid-based hyperedges  $E^G$ , though from different hypergraphs, are built on identical net connections—critical for fusing topological and geometric information in subsequent multi-view representation learning.

#### 4.2 Interpretable Subgraph Module

The interpretable subgraph module is designed to identify critical parts in the circuit hypergraph and guide the model to assign more attention to these parts.

**Multi-View Information Bottleneck.** We develop a Multi-View Information Bottleneck (MVIB) approach combining information from both cell-based netlist and grid-based layout data. After extracting hypergraphs  $H^C$  and  $H^G$ , IB learns bottleneck subgraphs for each view. Taking  $H^C$  as an example, the objective is to learn a bottleneck subgraph  $H^C_S$  by optimizing the following objective:

$$\max_{H_S^C} I(H^G; H_S^C) - \beta^C I(H^C; H_S^C \mid H^G), \tag{4}$$

where  $\beta^C$  controls compression-relevance trade-off. A similar formulation applies for  $H_S^G$ .

**Bottleneck Subgraph Extractor.** Inspired by [11], we adopt a single extractor design for both hypergraph views. The extractor processes hypergraph  $H^C$  using a Hypergraph Neural Network to obtain node probabilities, modeled as  $p_{\theta}(H_S^C|H^C) = \prod_{v \in V^C} p_{\theta}(v \in V_S^C|H^C)$ . The HNN outputs probability vector  $\mathbf{p} \in [0,1]^{|V^C|}$ , enabling bottleneck subgraph extraction:

$$H_S^C = (\mathbf{M}^C, \mathbf{X}_S^C) = (\mathbf{M}^C, \mathbf{X}^C \odot \mathbf{p}), \tag{5}$$

where  $\mathbf{M}^C$  is the incidence matrix of  $H^C$ ,  $\mathbf{X}^C$  represents the node features, and  $\odot$  denotes the row-wise production. The bottleneck subgraph for the grid-based view  $H_S^G$  can then be extracted using the mapped probability vector in the same form as Eq. (5).

Node probabilities map between views through spatial relationships. For each node  $v^G$  in  $H^G$ , its probability is  $\mathbf{p}^*[v^G] = \max_{v^C \in \mathcal{N}(v^G)} \mathbf{p}[v^C]$ , where  $\mathcal{N}(v^G)$  denotes cell nodes associated with grid node  $v^G$ . This single-extractor design ensures bottleneck subgraph consistency across views while reducing complexity. The extracted subgraphs  $H_S^C$  and  $H_S^G$  preserve the most informative structures for congestion prediction, guided by the information bottleneck objective in Eq. (7).

**Bottleneck Subgraph Augmentation.** After extracting the bottleneck subgraphs, we leverage bottleneck subgraphs to enhance feature representations through dynamic reweighting:

$$H^C = (\mathbf{M}^C, \mathbf{X}^C \cdot (1 + \sigma(W^C[\mathbf{X}^C | | \mathbf{X}_S^C]))), \quad H^G = (\mathbf{M}^G, \mathbf{X}^G \cdot (1 + \sigma(W^G[\mathbf{X}^G | | \mathbf{X}_S^G]))), \quad (6)$$
 where  $W^C$ ,  $W^G$  are learnable weights,  $\sigma$  is the sigmoid function, and  $||$  represents concatenation. This mechanism enhances features based on bottleneck structure relevance, while residual connections ensure stable gradient flow and preserve structural information.

**Multi-View Information Bottleneck Loss.** The information bottleneck loss regularizes bottleneck subgraph embeddings. The objective is reformulated as:

$$\mathcal{L}_{MVIB} = -I(H_S^C; H_S^G) + \beta D_{SKL} \left( p_{\theta}(H_S^C \mid H^C) \parallel p_{\gamma}(H_S^G \mid H^G) \right), \tag{7}$$

where  $p_{\theta}$  and  $p_{\gamma}$  refer to bottleneck subgraph extractors,  $D_{SKL}$  denotes symmetrized KL divergence, and  $\beta$  controls the trade-off between terms. Derivations from Eq. (4) Eq.(7) are in Appendix A.

#### 4.3 Multi-View Representation Learning Module

Given the multi-view data available, we propose a Multi-View Heterogeneous Graph Neural Network (MV-HGNN) that processes and integrates cell-based and grid-based hypergraph representations through a two-step message passing mechanism.

**Node-to-Hyperedge Message Passing.** For both cell-based and grid-based hypergraphs, we first aggregate node features within each hyperedge separately:

$$h_e^C = \sum_{v \in \mathcal{V}^C(e)} W_v^C h_v^C, \quad h_e^G = \sum_{v \in \mathcal{V}^G(e)} W_v^G h_v^G, \tag{8}$$

where  $h_e^C$ ,  $h_e^G$  are intermediate hyperedge embeddings,  $\mathcal{V}^{\mathcal{C}}(e)$ ,  $\mathcal{V}^{\mathcal{G}}(e)$  denote nodes in respective hyperedges, and  $W_v^C$ ,  $W_v^G$  can transform features into a common semantic space.

The net-based hyperedge embedding is then obtained by first concatenating these intermediate embeddings followed by a non-linear transformation:

$$h_e^N = \sigma(W_e^N[h_e^C||h_e^G]),$$
 (9)

 $h_e^N = \sigma(W_e^N[h_e^C||h_e^G]), \tag{9}$  where  $h_e^N$  represents the actual net-based hyperedge embedding that captures both topological and geometric information.

Hyperedge-to-Node Message Passing. The second step updates node embeddings by aggregating information from different sources. For cell-based nodes:

$$\hat{h}_{v}^{C} = \sum_{e \in \mathcal{E}^{C}(v)} W_{e}^{C} h_{e}^{C}, \quad \hat{h}_{v}^{N} = \sum_{e \in \mathcal{E}^{N}(v)} W_{e}^{N} h_{e}^{N},$$
(10)

where  $\hat{h}_v^C$ ,  $\hat{h}_v^N$  are intermediate embeddings from respective hyperedges,  $\mathcal{E}^C(v)$ ,  $\mathcal{E}^N(v)$  denote hyperedge sets containing node v. The final cell-based node embedding is obtained through concatenation and non-linear transformation:

$$h_v^{C'} = \sigma(W_v^{C'}[\hat{h}_v^C||\hat{h}_v^N]). \tag{11}$$

For grid-based nodes, we similarly aggregate information from spatially adjacent nodes and use the previously computed net-based hyperedge information:  $\hat{h}_v^G = \sum_{u \in \mathcal{N}^{\mathcal{G}}(v)} W_u^G h_u^G$ , where  $\mathcal{N}^{\mathcal{G}}(v)$  represents spatially adjacent grid nodes. The final grid-based embedding:

$$h_v^{G'} = \sigma(W_v^{G'}[\hat{h}_v^G | \hat{h}_v^S)). \tag{12}$$

After L message passing layers, final node embeddings serve two purposes: downstream congestion prediction and generating subgraph embeddings for contrastive learning. The subgraph embeddings are derived from previously identified bottleneck subgraphs:

$$h_S^C = \operatorname{Aggregate}(\{h_v^{C'} \mid v \in V_S^C\}), \quad h_S^G = \operatorname{Aggregate}(\{h_v^{G'} \mid v \in V_S^G\}).$$
 (13)

 $h_S^C = \operatorname{Aggregate}(\{h_v^{C'} \mid v \in V_S^C\}), \quad h_S^G = \operatorname{Aggregate}(\{h_v^{G'} \mid v \in V_S^G\}). \tag{13}$  This symmetric design facilitates effective congestion prediction for both views while maintaining the inherent characteristics of each representation.

Contrastive Loss. To enhance and align the interaction between cell-based and grid-based information, we employ contrastive learning. The contrastive loss is defined as:

$$\mathcal{L}_{\text{cont}} = -\sum_{i=1}^{N} \log \frac{\exp(\sin(h_{S_i}^C, h_{S_i}^G)/\tau)}{\sum_{i=1}^{N} \exp(\sin(h_{S_i}^C, h_{S_i}^G)/\tau)},$$
(14)

where  $h_{S_i}^C$ ,  $h_{S_i}^G$  form positive pairs from the same input,  $h_{S_j}^G$  represents negative samples, sim(a,b) denotes cosine similarity, and  $\tau$  controls similarity distribution sharpness.

#### 4.4 **Prediction Module**

Unlike previous methods that can only produce predictions in either the cell view or the grid view at once, our method's prediction module can output predictions in both scenarios simultaneously.

**Prediction.** In the prediction, we obtain both  $h_v^C$ , the cell-based node embedding, and  $h_v^G$ , the grid-based node embedding. Therefore, we use two MLPs,  $f^C$  and  $f^G$ , to map the two embeddings to the node congestion prediction results for both views:  $\hat{y}_v^C = f^C(h_v^C)$ ,  $\hat{y}_v^G = f^G(h_v^G)$ , where  $\hat{y}_v^C$  and  $\hat{y}_v^G$  represent the predicted node congestion values for the cell and grid views, respectively.

**Total Loss.** The overall loss combines contrastive (refer to Eq.(14)), supervised (refer to Eq.(2)), and information bottleneck losses (refer to Eq.(7)) to optimize the model.

$$\mathcal{L}_{\text{total}} = \mathcal{L}_{\text{cont}} + \mathcal{L}_{\text{IB}} + \mathcal{L}_{\text{sup}}. \tag{15}$$

**Time Complexity.** The overall complexity is  $O((|V_C| \times |E_C| + |V_G| \times |E_G|) \times D \times L)$ , where  $|V_C|$  and  $|V_C|$  represent the number of cell and grid nodes,  $|E_C|$  and  $|E_G|$  represent their respective hyperedges, D is the hidden dimension, and L is the number of layers.

Table 1: Placement-level results on All Datasets for both Cell- and Grid-based View. The best in **bold** and the second best underlined.

View	Model		ISPD2015-B						ISPD2013	5-F				CircuitNet-	N28	
VICW		NMAE↓	NRMS↓	Pearson <sup>†</sup>	Spearman <sup>†</sup>	Kendall↑	NMAE↓	NRMS↓	Pearson <sup>↑</sup>	Spearman <sup>†</sup>	Kendall↑	NMAE↓	NRMS↓	Pearson <sup>†</sup>	Spearman <sup>†</sup>	Kendall↑
	GCN	0.038	0.044	0.547	0.498	0.421	0.051	0.058	0.344	0.336	0.309	0.045	0.051	0.516	0.438	0.319
	GAT	0.039	0.045	0.531	0.517	0.463	0.050	0.057	0.351	0.342	0.298	0.046	0.051	0.513	0.447	0.321
Cell-	HGNN	0.036	0.042	0.577	0.553	0.476	0.045	0.052	0.410	0.366	0.309	0.044	0.048	0.552	0.468	0.332
based	CircuitGNN	0.034	0.040	0.598	0.611	0.487	0.046	0.053	0.402	0.378	0.316	0.040	0.043	0.609	0.500	0.368
baseu	LHNN	0.033	0.038	0.629	0.627	0.502	0.043	0.049	0.448	0.384	0.364	0.039	0.043	0.617	0.509	0.366
	DE-HNN	0.032	0.037	0.645	0.632	0.520	0.042	0.048	0.467	0.395	0.381	0.038	0.042	0.638	0.511	0.374
	MIHC (Ours)	0.029	0.034	0.687	0.689	0.574	0.035	0.041	0.524	0.512	0.447	0.036	0.039	0.661	0.522	0.396
	GCN	0.043	0.049	0.405	0.162	0.137	0.046	0.053	0.357	0.152	0.131	0.052	0.053	0.417	0.399	0.312
	GAT	0.044	0.050	0.398	0.144	0.141	0.048	0.055	0.331	0.137	0.116	0.052	0.054	0.411	0.405	0.323
	HGNN	0.040	0.046	0.451	0.184	0.142	0.043	0.050	0.352	0.147	0.121	0.051	0.052	0.442	0.424	0.331
Grid-	RouteNet	0.038	0.045	0.522	0.198	0.157	0.042	0.050	0.362	0.161	0.137	0.047	0.049	0.541	0.501	0.373
	CircuitGNN	0.037	0.043	0.561	0.201	0.164	0.042	0.049	0.364	0.162	0.134	0.047	0.048	0.547	0.508	0.371
based	CircuitFormer	0.034	0.040	0.649	0.231	0.169	0.038	0.045	0.453	0.196	0.165	0.044	0.046	0.622	0.526	0.384
	LHNN	0.033	0.040	0.651	0.252	0.217	0.037	0.044	0.464	0.221	0.182	0.043	0.044	0.646	0.533	0.389
	Lay-Net	0.031	0.037	0.667	0.301	0.248	0.035	0.042	0.484	0.256	0.208	0.041	0.043	0.671	0.558	0.406
	MIHC (Ours)	0.030	0.036	0.675	0.297	0.252	0.032	0.039	0.503	0.271	0.227	0.040	0.041	0.682	0.572	0.402

Table 2: Design-level results on ISPD2015-B and ISPD2015-F for both Cell- and Grid-based View. The best in **bold** and the second best underlined.

Direction	View	Model			ISPD2015	5-B				ISPD2015	5-F	
Direction	view	Model	NMAE↓	NRMS↓	Pearson <sup>†</sup>	Spearman <sup>†</sup>	Kendall↑	NMAE↓	NRMS↓	Pearson <sup>↑</sup>	Spearman <sup>†</sup>	Kendall↑
		CircuitGNN	0.058	0.064	0.376	0.335	0.248	0.071	0.077	0.343	0.304	0.218
	Cell-	LHNN	0.054	0.060	0.398	0.355	0.265	0.067	0.073	0.368	0.321	0.235
	based	DE-HNN	0.051	0.057	0.415	0.372	0.282	0.063	0.069	0.385	0.342	0.252
$A{\rightarrow}B$		MIHC (Ours)	0.048	0.053	0.448	0.405	0.302	0.059	0.065	0.414	0.375	0.277
А→В		CircuitGNN	0.061	0.067	0.366	0.158	0.132	0.074	0.080	0.331	0.148	0.122
	Grid-	LHNN	0.057	0.063	0.389	0.172	0.145	0.070	0.076	0.349	0.162	0.135
	based	Lay-Net	0.053	0.059	0.411	0.192	0.165	0.064	0.070	0.394	0.200	0.174
		MIHC (Ours)	0.051	0.057	0.436	0.218	0.188	0.064	0.069	0.405	0.201	0.167
		CircuitGNN	0.063	0.068	0.351	0.325	0.232	0.075	0.081	0.337	0.293	0.205
	Cell-	LHNN	0.058	0.065	0.379	0.347	0.246	0.070	0.076	0.354	0.315	0.222
	based	DE-HNN	0.053	0.058	0.405	0.365	0.269	0.065	0.071	0.378	0.336	0.238
$B \rightarrow A$		MIHC (Ours)	0.049	0.055	0.428	0.384	0.281	0.062	0.067	0.399	0.357	0.262
Б→А		CircuitGNN	0.064	0.070	0.348	0.148	0.122	0.077	0.083	0.318	0.138	0.112
	Grid-	LHNN	0.060	0.066	0.369	0.162	0.135	0.073	0.079	0.337	0.152	0.125
	based	Lay-Net	0.055	0.061	0.392	0.197	0.179	0.068	0.073	0.367	0.191	0.152
		MIHC (Ours)	0.054	0.059	0.415	0.202	0.175	0.067	0.072	0.388	0.182	0.168

## 5 Experiments

In this section, we evaluate MIHC through comprehensive experiments designed to address four key research questions:

**RQ1:** How does MIHC's circuit congestion prediction accuracy compare to state-of-the-art methods?

**RQ2:** What is the MIHC's interpretability performance?

**RQ3:** What is the impact of MIHC's core design components on its overall performance?

**RQ4:** How sensitive is MIHC's performance to parameter variations?

## 5.1 Experimental Setup

**Datasets.** For chip congestion prediction, we evaluate our method on two public datasets: ISPD2015 [2] and CircuitNet-N28 [3]. ISPD2015 is divided into two variants: ISPD2015-Balanced (ISPD2015-B), which excludes extremely large superblue circuits, and ISPD2015-Full (ISPD2015-F), which includes them, allowing us to assess our model's performance on data imbalance challenges. CircuitNet-N28 contains over 10,000 samples (compared to ISPD2015's approximately 500), providing a more comprehensive test of our model's generalizability across diverse circuit designs.

To rigorously evaluate generalization capability, we employ two data partitioning strategies: (1) Placement-level split, where different placement solutions from the same design appear in both training and test sets, and (2) Design-level split, where training and test sets contain completely different circuit designs with no overlap. The placement-level split follows our standard 7:3 train-test ratio, while the design-level split involves bidirectional evaluation  $(A \rightarrow B \text{ and } B \rightarrow A)$  on carefully partitioned design groups. Detailed partitioning strategies are presented in Appendix C.5.

For explainable GAD task, we use MNIST0 and MNIST1 datasets [11].

**Baselines.** There are two aspects of prediction tasks: cell-based prediction and grid-based prediction. To comprehensively evaluate our model, we first employ several classical graph learning models as

baselines: GCN [8], GAT [19], and HGNN [7]. Furthermore, we compare with specialized circuit-oriented models: CircuitGNN [24] and LHNN [20], which are capable of handling both cell-based and grid-based predictions; DE-HNN [14], which focuses exclusively on cell-based prediction; and RouteNet [22], CircuitFormer [29] and Lay-Net [28], which specifically target grid-based prediction. To illustrate the usefulness of the model interpretability module, we chose GCN + GNNExplainer [25], GAT + GNNExplainer and SIGNET [11] as baselines.

**Evaluation Metrics.** For chip congestion prediction, similar to [24], we employ both regression-based metrics (NMAE and NRMS) to measure prediction accuracy and ranking-based metrics (Pearson, Spearman, and Kendall correlations) to assess prediction quality; while in interpretability module test, since the downstream task is a classification task, ACC, Precision, Recall, F1, and AUC are used to measure the accuracy of the classification.

Further details about datasets and our experiment settings are presented in Appendix C.

#### **5.2** Chip Congestion Prediction Results (RQ1)

We present comprehensive evaluation results under both placement-level and design-level settings. The placement-level results are shown in Table 1 and design-level results are presented in Table 2, both with the best in **bold** and the second best <u>underlined</u> (More details in Appendix D.1). Given that our data encompasses both cell and grid views, we assess the validity and rationality of our model across these dual views by comparing prediction accuracy against their respective state-of-the-art (SOTA) counterparts.

#### 5.2.1 Placement-level Results

As shown in Table 1, for ISPD2015-B, MIHC outperforms the SOTA method DE-HNN with 9.37% reduction in NMAE and 6.51% improvement in Pearson correlation at the cell level, and surpasses Lay-Net with 3.23% reduction in NMAE and 1.20% improvement in Pearson correlation at the grid level. On the more challenging ISPD2015-F with extremely large circuits, MIHC achieves even more significant gains: 16.67% reduction in NMAE and 12.21% improvement in Pearson correlation compared to DE-HNN at the cell level, and 8.57% reduction in NMAE and 3.93% improvement in Pearson correlation over Lay-Net at the grid level. These results demonstrate MIHC's robustness when handling imbalanced data distributions. The CircuitNet-N28 results, based on over 10,000 diverse samples, further confirm MIHC's generalizability with 5.26% NMAE reduction and 3.60% Pearson improvement compared to DE-HNN at the cell level, and 2.44% NMAE reduction and 1.64% Pearson improvement over Lay-Net at the grid level. This consistent performance across a substantially larger dataset validates our method's universal applicability for congestion prediction in real-world VLSI design environments.

## 5.2.2 Design-level Results

To rigorously evaluate generalization to entirely unseen circuit designs, we conduct additional experiments following the design-level split setting (detailed setup in Appendix C.5), where training and test sets contain completely different circuit designs with no overlap. As shown in Table 2, this setting presents significantly more challenging conditions with substantial performance degradation across all methods. Despite these challenges, MIHC maintains superior performance over baselines in the vast majority of metrics. For ISPD2015-B, MIHC outperforms DE-HNN with 7.55% reduction in cell-based NMAE and 5.68% improvement in Pearson correlation in the B $\rightarrow$ A experiments, while achieving 5.87% Pearson improvement in grid-based prediction over Lay-Net. For ISPD2015-F, MIHC achieves 6.35% cell-based NMAE reduction and 7.53% Pearson improvement in the A $\rightarrow$ B direction. These results provide strong evidence that our method achieves genuine generalization capability rather than simply memorizing design-specific characteristics, offering a realistic evaluation for real-world deployment scenarios.

#### 5.3 Explainability Results (RQ2)

To validate the effectiveness of our model's explainability module, we examine its capability to identify important structures in chip congestion prediction scenarios. As demonstrated in Figure 2, our bottleneck subgraph successfully captures critical congestion regions, and MIHC achieves

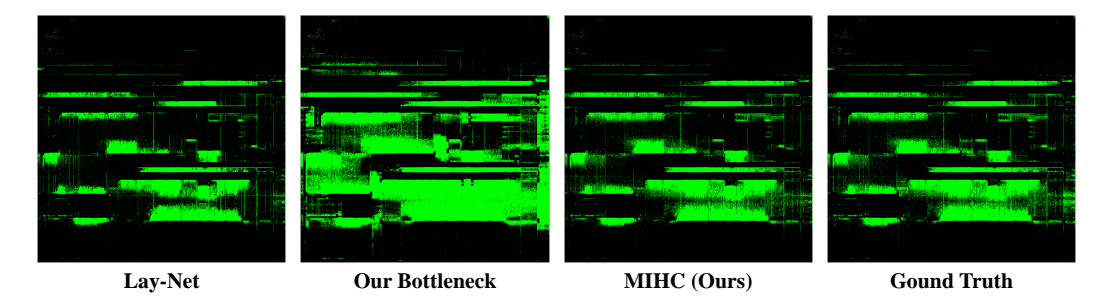


Figure 2: Visualization of heat maps on ISPD2015/mgc\_superblue16\_a design showing Lay-Net, our bottleneck subgraph, MIHC (Ours), and ground truth congestion maps.

Table 3: Ablation Study of Model Modules on ISPD2015-B. The best in **bold**.

Model Variants			Cell-based Results	3		Grid-based Results				
	NMAE.	NRMS↓	Pearson↑	Spearman↑	Kendall↑	NMAE↓	NRMS↓	Pearson↑	Spearman↑	Kendall↑
HGNN	0.036	0.042	0.577	0.553	0.476	0.040	0.046	0.451	0.184	0.142
w/o MV-HGNN	0.036 (0.0%)	0.041 (+2.4%)	0.580 (+0.5%)	0.571 (+3.3%)	0.477 (+0.2%)	0.039 (+2.5%)	0.044 (+4.3%)	0.482 (+6.9%)	0.187 (+1.6%)	0.144 (+1.4%)
w/o ISM	0.031 (+13.9%)	0.036 (+14.3%)	0.654 (+13.3%)	0.643 (+16.3%)	0.536 (+12.6%)	0.033 (+17.5%)	0.039 (+15.2%)	0.652 (+44.6%)	0.263 (+42.9%)	0.231 (+62.7%)
Full Model	0.029 (+19.4%)	0.034 (+19.0%)	0.687 (+19.1%)	0.689 (+24.6%)	0.574 (+20.6%)	0.030 (+25.0%)	0.036 (+21.7%)	0.675 (+49.7%)	0.297 (+61.4%)	0.252 (+77.5%)

Table 4: Ablation Study of Different Loss Functions on ISPD2015-B.

Lo	ss Cor	npon	ents		Cell-based Results				Grid-based Results				
Cell	Grid	IB	Cont	NMAE↓	NRMS↓	Pearson <sup>†</sup>	Spearman <sup>†</sup>	Kendall↑	NMAE↓	NRMS↓	Pearson <sup>†</sup>	Spearman†	Kendall↑
_	×	×	Х	0.033	0.038	0.639	0.622	0.511	0.037	0.042	0.612	0.222	0.205
X	/	Х	Х	0.035 (-6.06%)	0.040 (-5.26%)	0.596 (-6.73%)	0.605 (-2.73%)	0.484 (-5.28%)	0.034 (+8.11%)	0.040 (+4.76%)	0.650 (+6.21%)	0.254 (+14.41%)	0.241 (+17.56%)
/	/	X	Х	0.031 (+6.06%)	0.036 (+5.26%)	0.659 (+3.13%)	0.658 (+5.79%)	0.550 (+7.63%)	0.033 (+10.81%)	0.039 (+7.14%)	0.661 (+8.01%)	0.264 (+18.92%)	0.243 (+18.54%)
/	/	X	/	0.030 (+9.09%)	0.036 (+5.26%)	0.662 (+3.60%)	0.660 (+6.11%)	0.554 (+8.41%)	0.033 (+10.81%)	0.038 (+9.52%)	0.666 (+8.82%)	0.269 (+21.17%)	0.246 (+20.00%)
/	/	/	Х	0.029 (+12.12%)	0.035 (+7.89%)	0.672 (+5.16%)	0.665 (+6.91%)	0.559 (+9.39%)	0.031 (+16.22%)	0.038 (+9.52%)	0.671 (+9.64%)	0.284 (+27.93%)	0.249 (+21.46%)
/	/	1	/	0.029 (+12.12%)	0.034 (+10.53%)	0.687 (+7.51%)	0.689 (+10.77%)	0.574 (+12.33%)	0.030 (+18.92%)	0.036 (+14.29%)	0.675 (+10.29%)	0.297 (+33.78%)	0.252 (+22.93%)

predictions that closely match the ground truth patterns, underscoring its superior interpretability. Additionally, the bottleneck subgraph heat map indicates that our IB bottleneck subgraph can be extracted to reveal regions relevant to the final prediction results. While node-level predictions identify congestion points, our Information Bottleneck identifies the critical local structures that cause these anomalies, revealing the structural patterns that contribute to surrounding node congestion rather than just detecting generic anomalies. This is particularly important in circuit design where congestion typically emerges from interactions between neighboring components rather than isolated elements. Due to the lack of publicly available datasets for interpretability in the EDA domain, we also briefly evaluated our model on the MNIST 0/1 dataset, where it demonstrated strong consistency across various metrics in Table 16. In comparison, baseline methods showed significant limitations: GAT+GNNExplainer suffered from low precision while SIGNET failed to capture comprehensive node relationships. These results, combined with the visual evidence from chip congestion heatmaps, confirm that MIHC not only delivers superior prediction accuracy but also provides meaningful explainability for practical VLSI design applications.

## 5.4 Ablation Study(RQ3)

In ablation studies, we conducted two sets of experiments on ISPD2015-B to evaluate: the contribution of different model modules (Table 3) and the impact of different loss functions (Table 4).

The ablation results of model modules in Table 3 reveal several important findings. First, removing the Multi-View Representation Learning Module (w/o MV-HGNN) results in performance similar to the basic HGNN but significantly worse than the Full Model, demonstrating the crucial role of multi-view information fusion. Second, excluding the Interpretable Subgraph Module (w/o ISM) yields better results than basic HGNN but still underperforms compared to the Full Model, with substantial decreases in correlation metrics (13.3% lower Pearson for cell-based results). Finally, the Full Model achieves optimal performance across all metrics by effectively combining ISM for critical information filtering with MV-HGNN for multi-view integration, showing impressive improvements over the baseline HGNN (19.1% Pearson improvement for cell-based results).

The comprehensive ablation results in Table 4 systematically demonstrate the effectiveness evaluation of different loss functions. The experimental results show that using both Cell and Grid Supervised loss consistently achieves better performance (NMAE=0.031 for cell-based, 0.033 for grid-based)

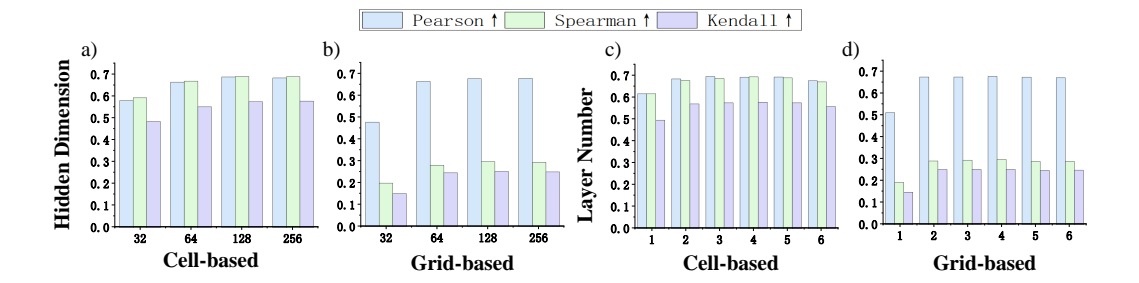


Figure 3: Hyperparameter sensitivity analysis: Impact of hidden dimensions (a,b) and MV-HGNN layer number (c,d) on cell-based and grid-based performance.

compared to single-view supervision (Cell-Sup only: 0.033, 0.037; Grid-Sup only: 0.035, 0.034), thus validating the fundamental importance of multi-view information fusion by using multi-view loss. Furthermore, through detailed comparative analysis, the removal of IB loss (w/o IB Loss) leads to substantial performance degradation (Pearson correlation decreases by 4.21% for cell-based results), confirming its crucial role in guiding the model to extract essential subgraph components.

## 5.5 Parameters Sensitivity(RQ4)

We conduct a comprehensive hyperparameter analysis of MIHC on ISPD2015-B, specifically examining the impact of Multi-View HGNN layer number (ranging from 1 to 6) and hidden dimensions (varying from 32 to 256) on model performance. As illustrated in Figure 3, MIHC demonstrates robust stability across different hyperparameter configurations. However, notable performance degradation occurs in two specific configurations: when the model is configured with a single Multi-View HGNN layer or when the hidden dimension is set to 32. These significant performance drops can be attributed to insufficient model capacity, as either a single layer or a small hidden dimension proves inadequate for learning the complex hierarchical features and relationships inherent in the data.

## 6 Conclusion

This paper presents MIHC, a novel interpretable hypergraph neural network for circuit congestion prediction. Through its balanced multi-view hypergraph architecture with net-based bridging, MIHC achieves effective fusion of netlist and layout information, providing a comprehensive understanding of circuit characteristics. The incorporation of a subgraph Information Bottleneck mechanism further enhances the model by identifying critical subgraphs correlated with congestion patterns and leveraging this selective information to improve prediction accuracy. Our comprehensive experiments demonstrate MIHC's superior performance compared to existing methods, achieving significant improvements in both cell-based and grid-based prediction tasks. This synergistic combination of balanced multi-view information fusion and interpretable bottleneck analysis represents a meaningful advancement in trustworthy Electronic Design Automation, establishing a foundation for future interpretable machine learning approaches in integrated circuit design.

**Limitations.** While MIHC achieves significant performance improvements, there remain areas for enhancement. The Information Bottleneck mechanism, though effective for interpretability, introduces computational complexity that could be optimized with more efficient algorithms. Additionally, our comparative analysis between ISPD2015-B and ISPD2015-F indicates that performance on imbalanced datasets, while still superior to baselines, presents opportunities for improvement—a challenge shared across current congestion prediction approaches. Future work will address these aspects while maintaining MIHC's interpretability and prediction accuracy advantages.

**Broader impacts.** Our interpretable hypergraph model enhances EDA performance with limited impact. There is a minimal possibility that without proper validation, over-reliance risks erroneous decisions in chip design.

## Acknowledgements

The authors H.P., P.Z., X.X., and P.B. acknowledge the support by the U.S. Army Research Office (ARO) under Grant No. W911NF-23-1-0111, the National Science Foundation (NSF) under the NSF Award 2243104 under the Center for Complex Particle Systems (COMPASS), the Career Award CPS-1453860, Career Award 2337412, CNS-1932620, and NSF Mid-Career Advancement Award BCS-2527046, the Defense Advanced Research Projects Agency (DARPA) Young Faculty Award and DARPA Director Fellowship Award under Grant Number N66001-17-1-4044, Intel faculty awards and a Northrop Grumman grant. P.B. is also grateful to National Institute of Health (NIH) for the grants R01 AG 079957 "Interpretable machine learning to synergize brain age estimation and neuroimaging genetics" and RF1 AG 082201 "Neurovascular calcification and ADRD in two nonindustrial Native American populations". It was a wonderful experience designing and writing the grant application entitled "Neurovascular calcification and ADRD in two nonindustrial Native American populations" and awarded under RF1 AG 082201. The authors Z.Z. and X.L. acknowledge the support by NSFC (No. 72171229), the MOE Project of Key Research Institute of Humanities and Social Sciences (No. 22JJD110001), and Big Data and Responsible Artificial Intelligence for National Governance, RUC. The views, opinions, and/or findings in this article are those of the authors and should not be interpreted as official views or policies of the Department of Defense, the National Institute of Health or the National Science Foundation.

## References

- [1] Kyeonghyeon Baek, Hyunbum Park, Suwan Kim, Kyumyung Choi, and Taewhan Kim. Pin accessibility and routing congestion aware DRC hotspot prediction using graph neural network and U-Net. In *Proceedings of the 41st IEEE/ACM International Conference on Computer-Aided Design*, pages 1–9, October 2022.
- [2] Ismail S. Bustany, David Chinnery, Joseph R. Shinnerl, and Vladimir Yutsis. ISPD 2015 benchmarks with fence regions and routing blockages for detailed-routing-driven placement. In Proceedings of the 2015 Symposium on International Symposium on Physical Design, pages 157–164, March 2015.
- [3] Zhuomin Chai, Yuxiang Zhao, Wei Liu, Yibo Lin, Runsheng Wang, and Ru Huang. CircuitNet: An open-source dataset for machine learning in VLSI CAD applications with improved domain-specific evaluation metric and learning strategies. *IEEE Transactions on Computer-Aided Design of Integrated Circuits and Systems*, 42(12):5034–5047, 2023.
- [4] Amur Ghose, Vincent Zhang, Yingxue Zhang, Dong Li, Wulong Liu, and Mark Coates. Generalizable cross-graph embedding for GNN-based congestion prediction. In 2021 IEEE/ACM International Conference On Computer Aided Design (ICCAD), pages 1–9. IEEE, November 2021.
- [5] Amur Ghose, Vincent Zhang, Yingxue Zhang, Dong Li, Wulong Liu, and Mark Coates. Generalizable cross-graph embedding for GNN-based congestion prediction. In 2021 IEEE/ACM International Conference on Computer Aided Design (ICCAD), pages 1–9. IEEE, November 2021.
- [6] Hao Gu, Youwen Wang, Xinglin Zheng, Keyu Peng, Ziran Zhu, Jianli Chen, and Jun Yang. Dual multimodal fusions with convolution and transformer layers for VLSI congestion prediction. *IEEE Transactions on Computer-Aided Design of Integrated Circuits and Systems*, 2024.
- [7] Sunwoo Kim, Soo Yong Lee, Yue Gao, Alessia Antelmi, Mirko Polato, and Kijung Shin. A survey on hypergraph neural networks: An in-depth and step-by-step guide. In *Proceedings of the 30th ACM SIGKDD Conference on Knowledge Discovery and Data Mining*, pages 6534–6544, August 2024.
- [8] Thomas N Kipf and Max Welling. Semi-supervised classification with graph convolutional networks. *arXiv preprint arXiv:1609.02907*, 2016.
- [9] Robert Kirby, Saad Godil, Rajarshi Roy, and Bryan Catanzaro. Congestionnet: Routing congestion prediction using deep graph neural networks. In 2019 IFIP/IEEE 27th International Conference on Very Large Scale Integration (VLSI-SoC), pages 217–222. IEEE, October 2019.

- [10] Biao Liu, Congyu Qiao, Ning Xu, Xin Geng, Ziran Zhu, and Jun Yang. Variational label-correlation enhancement for congestion prediction. In 2024 29th Asia and South Pacific Design Automation Conference (ASP-DAC), pages 466–471. IEEE, January 2024.
- [11] Yixin Liu, Kaize Ding, Qinghua Lu, Fuyi Li, Leo Yu Zhang, and Shirui Pan. Towards self-interpretable graph-level anomaly detection. *Advances in Neural Information Processing Systems*, 36, 2024.
- [12] Daniela Sánchez Lopera, Lorenzo Servadei, Gamze Naz Kiprit, Souvik Hazra, Robert Wille, and Wolfgang Ecker. A survey of graph neural networks for electronic design automation. In 2021 ACM/IEEE 3rd Workshop on Machine Learning for CAD (MLCAD), pages 1–6. IEEE, August 2021.
- [13] Dongsheng Luo, Wei Cheng, Dongkuan Xu, Wenchao Yu, Bo Zong, Haifeng Chen, and Xiang Zhang. Parameterized explainer for graph neural network. *Advances in neural information processing systems*, 33:19620–19631, 2020.
- [14] Zhishang Luo, Truong Son Hy, Puoya Tabaghi, Michaël Defferrard, Elahe Rezaei, Ryan M. Carey, Rhett Davis, Rajeev Jain, and Yusu Wang. DE-HNN: An effective neural model for circuit netlist representation. In *International Conference on Artificial Intelligence and Statistics*, pages 4258–4266. PMLR, April 2024.
- [15] Almitra Pradhan and Ranga Vemuri. Efficient synthesis of a uniformly spread layout aware Pareto surface for analog circuits. In 2009 22nd International Conference on VLSI Design, pages 131–136. IEEE, January 2009.
- [16] Mukesh Ranjan, Wim Verhaegen, Anuradha Agarwal, Hemanth Sampath, Ranga Vemuri, and Georges Gielen. Fast, layout-inclusive analog circuit synthesis using pre-compiled parasitic-aware symbolic performance models. In *Proceedings Design, Automation and Test in Europe Conference and Exhibition*, volume 1, pages 604–609. IEEE, February 2004.
- [17] Naftali Tishby, Fernando C Pereira, and William Bialek. The information bottleneck method. arXiv preprint physics/0004057, 2000.
- [18] Peter Vancorenland, Geert Van der Plas, Michiel Steyaert, Georges Gielen, and W. Sansen. A layout-aware synthesis methodology for RF circuits. In *IEEE/ACM International Conference on Computer Aided Design (ICCAD)*, pages 358–362. IEEE, November 2001.
- [19] Petar Veličković, Guillem Cucurull, Arantxa Casanova, Adriana Romero, Pietro Lio, and Yoshua Bengio. Graph attention networks. *arXiv preprint arXiv:1710.10903*, 2017.
- [20] Bowen Wang, Guibao Shen, Dong Li, Jianye Hao, Wulong Liu, Yu Huang, Hongzhong Wu, Yibo Lin, Guangyong Chen, and Pheng Ann Heng. Lhnn: Lattice hypergraph neural network for VLSI congestion prediction. In *Proceedings of the 59th ACM/IEEE Design Automation Conference*, pages 1297–1302. ACM/IEEE, July 2022.
- [21] Xiongye Xiao, Gengshuo Liu, Gaurav Gupta, Defu Cao, Shixuan Li, Yaxing Li, Tianqing Fang, Mingxi Cheng, and Paul Bogdan. Neuro-inspired information-theoretic hierarchical perception for multimodal learning. In *The Twelfth International Conference on Learning Representations*, 2024.
- [22] Zhiyao Xie, Yu-Hung Huang, Guan-Qi Fang, Haoxing Ren, Shao-Yun Fang, Yiran Chen, and Jiang Hu. RouteNet: Routability prediction for mixed-size designs using convolutional neural network. In 2018 IEEE/ACM International Conference on Computer-Aided Design (ICCAD), pages 1–8. IEEE, November 2018.
- [23] Yuankun Xue and Paul Bogdan. Constructing compact causal mathematical models for complex dynamics. In *Proceedings of the 8th International Conference on Cyber-Physical Systems*, pages 97–107, 2017.
- [24] Shuwen Yang, Zhihao Yang, Dong Li, Yingxueff Zhang, Zhanguang Zhang, Guojie Song, and Jianye Hao. Versatile multi-stage graph neural network for circuit representation. *Advances in Neural Information Processing Systems*, 35:20313–20324, 2022.

- [25] Zhitao Ying, Dylan Bourgeois, Jiaxuan You, Marinka Zitnik, and Jure Leskovec. Gnnexplainer: Generating explanations for graph neural networks. *Advances in neural information processing systems*, 32, 2019.
- [26] Cunxi Yu and Zhiru Zhang. Painting on placement: Forecasting routing congestion using conditional generative adversarial nets. In *Proceedings of the 56th Annual Design Automation Conference*, pages 1–6, June 2019.
- [27] Yuxiang Zhao, Zhuomin Chai, Yibo Lin, Runsheng Wang, and Ru Huang. HybridNet: Dual-branch fusion of geometrical and topological views for VLSI congestion prediction. In 2023 International Symposium of Electronics Design Automation (ISEDA), pages 314–316. IEEE, May 2023.
- [28] Su Zheng, Lancheng Zou, Peng Xu, Siting Liu, Bei Yu, and Martin Wong. Lay-Net: Grafting netlist knowledge on layout-based congestion prediction. In 2023 IEEE/ACM International Conference on Computer Aided Design (ICCAD), pages 1–9. IEEE, October 2023.
- [29] Jialv Zou, Xinggang Wang, Jiahao Guo, Wenyu Liu, Qian Zhang, and Chang Huang. Circuit as set of points. *Advances in Neural Information Processing Systems*, 36, 2024.

## **NeurIPS Paper Checklist**

#### 1. Claims

Question: Do the main claims made in the abstract and introduction accurately reflect the paper's contributions and scope?

Answer: [Yes]

Justification: The main claims made in the abstract and introduction accurately reflect the paper's contributions and scope. See the Abstract and Introduction sections.

#### Guidelines:

- The answer NA means that the abstract and introduction do not include the claims made in the paper.
- The abstract and/or introduction should clearly state the claims made, including the contributions made in the paper and important assumptions and limitations. A No or NA answer to this question will not be perceived well by the reviewers.
- The claims made should match theoretical and experimental results, and reflect how much the results can be expected to generalize to other settings.
- It is fine to include aspirational goals as motivation as long as it is clear that these goals are not attained by the paper.

#### 2. Limitations

Question: Does the paper discuss the limitations of the work performed by the authors?

Answer: [Yes]

Justification: The limitation of the work is discussed in the Conclusion section.

#### Guidelines:

- The answer NA means that the paper has no limitation while the answer No means that the paper has limitations, but those are not discussed in the paper.
- The authors are encouraged to create a separate "Limitations" section in their paper.
- The paper should point out any strong assumptions and how robust the results are to violations of these assumptions (e.g., independence assumptions, noiseless settings, model well-specification, asymptotic approximations only holding locally). The authors should reflect on how these assumptions might be violated in practice and what the implications would be.
- The authors should reflect on the scope of the claims made, e.g., if the approach was only tested on a few datasets or with a few runs. In general, empirical results often depend on implicit assumptions, which should be articulated.
- The authors should reflect on the factors that influence the performance of the approach. For example, a facial recognition algorithm may perform poorly when image resolution is low or images are taken in low lighting. Or a speech-to-text system might not be used reliably to provide closed captions for online lectures because it fails to handle technical jargon.
- The authors should discuss the computational efficiency of the proposed algorithms and how they scale with dataset size.
- If applicable, the authors should discuss possible limitations of their approach to address problems of privacy and fairness.
- While the authors might fear that complete honesty about limitations might be used by reviewers as grounds for rejection, a worse outcome might be that reviewers discover limitations that aren't acknowledged in the paper. The authors should use their best judgment and recognize that individual actions in favor of transparency play an important role in developing norms that preserve the integrity of the community. Reviewers will be specifically instructed to not penalize honesty concerning limitations.

## 3. Theory assumptions and proofs

Question: For each theoretical result, does the paper provide the full set of assumptions and a complete (and correct) proof?

Answer: [Yes]

Justification: For all theoretical results, the paper provides the corresponding proofs in the appendix.

#### Guidelines:

- The answer NA means that the paper does not include theoretical results.
- All the theorems, formulas, and proofs in the paper should be numbered and cross-referenced.
- All assumptions should be clearly stated or referenced in the statement of any theorems.
- The proofs can either appear in the main paper or the supplemental material, but if they appear in the supplemental material, the authors are encouraged to provide a short proof sketch to provide intuition.
- Inversely, any informal proof provided in the core of the paper should be complemented by formal proofs provided in appendix or supplemental material.
- Theorems and Lemmas that the proof relies upon should be properly referenced.

## 4. Experimental result reproducibility

Question: Does the paper fully disclose all the information needed to reproduce the main experimental results of the paper to the extent that it affects the main claims and/or conclusions of the paper (regardless of whether the code and data are provided or not)?

Answer: [Yes]

Justification: The paper fully discloses all the information needed to reproduce the main experimental results in the paper. See the Experiments section.

#### Guidelines:

- The answer NA means that the paper does not include experiments.
- If the paper includes experiments, a No answer to this question will not be perceived
  well by the reviewers: Making the paper reproducible is important, regardless of
  whether the code and data are provided or not.
- If the contribution is a dataset and/or model, the authors should describe the steps taken to make their results reproducible or verifiable.
- Depending on the contribution, reproducibility can be accomplished in various ways. For example, if the contribution is a novel architecture, describing the architecture fully might suffice, or if the contribution is a specific model and empirical evaluation, it may be necessary to either make it possible for others to replicate the model with the same dataset, or provide access to the model. In general, releasing code and data is often one good way to accomplish this, but reproducibility can also be provided via detailed instructions for how to replicate the results, access to a hosted model (e.g., in the case of a large language model), releasing of a model checkpoint, or other means that are appropriate to the research performed.
- While NeurIPS does not require releasing code, the conference does require all submissions to provide some reasonable avenue for reproducibility, which may depend on the nature of the contribution. For example
  - (a) If the contribution is primarily a new algorithm, the paper should make it clear how to reproduce that algorithm.
  - (b) If the contribution is primarily a new model architecture, the paper should describe the architecture clearly and fully.
- (c) If the contribution is a new model (e.g., a large language model), then there should either be a way to access this model for reproducing the results or a way to reproduce the model (e.g., with an open-source dataset or instructions for how to construct the dataset).
- (d) We recognize that reproducibility may be tricky in some cases, in which case authors are welcome to describe the particular way they provide for reproducibility. In the case of closed-source models, it may be that access to the model is limited in some way (e.g., to registered users), but it should be possible for other researchers to have some path to reproducing or verifying the results.

## 5. Open access to data and code

Question: Does the paper provide open access to the data and code, with sufficient instructions to faithfully reproduce the main experimental results, as described in supplemental material?

Answer: [Yes]

Justification: We provide available sources in an anonymous GitHub repository to reproduce the experimental results.

#### Guidelines:

- The answer NA means that paper does not include experiments requiring code.
- Please see the NeurIPS code and data submission guidelines (https://nips.cc/public/guides/CodeSubmissionPolicy) for more details.
- While we encourage the release of code and data, we understand that this might not be possible, so "No" is an acceptable answer. Papers cannot be rejected simply for not including code, unless this is central to the contribution (e.g., for a new open-source benchmark).
- The instructions should contain the exact command and environment needed to run to reproduce the results. See the NeurIPS code and data submission guidelines (https://nips.cc/public/guides/CodeSubmissionPolicy) for more details.
- The authors should provide instructions on data access and preparation, including how
  to access the raw data, preprocessed data, intermediate data, and generated data, etc.
- The authors should provide scripts to reproduce all experimental results for the new proposed method and baselines. If only a subset of experiments are reproducible, they should state which ones are omitted from the script and why.
- At submission time, to preserve anonymity, the authors should release anonymized versions (if applicable).
- Providing as much information as possible in supplemental material (appended to the paper) is recommended, but including URLs to data and code is permitted.

## 6. Experimental setting/details

Question: Does the paper specify all the training and test details (e.g., data splits, hyper-parameters, how they were chosen, type of optimizer, etc.) necessary to understand the results?

Answer: [Yes]

Justification: We specify all the training and test details necessary to understand the results. See the Experiments section.

#### Guidelines:

- The answer NA means that the paper does not include experiments.
- The experimental setting should be presented in the core of the paper to a level of detail that is necessary to appreciate the results and make sense of them.
- The full details can be provided either with the code, in appendix, or as supplemental material.

## 7. Experiment statistical significance

Question: Does the paper report error bars suitably and correctly defined or other appropriate information about the statistical significance of the experiments?

Answer: [Yes]

Justification: We have verified our experiment results under different settings, which can be seen in our Experiment section and Appendix. According to the baselines, our work follows the same experiment settings and we believe the experiment results in the paper can accurately reflect the performance of our work.

- The answer NA means that the paper does not include experiments.
- The authors should answer "Yes" if the results are accompanied by error bars, confidence intervals, or statistical significance tests, at least for the experiments that support the main claims of the paper.

- The factors of variability that the error bars are capturing should be clearly stated (for example, train/test split, initialization, random drawing of some parameter, or overall run with given experimental conditions).
- The method for calculating the error bars should be explained (closed form formula, call to a library function, bootstrap, etc.)
- The assumptions made should be given (e.g., Normally distributed errors).
- It should be clear whether the error bar is the standard deviation or the standard error
  of the mean.
- It is OK to report 1-sigma error bars, but one should state it. The authors should preferably report a 2-sigma error bar than state that they have a 96% CI, if the hypothesis of Normality of errors is not verified.
- For asymmetric distributions, the authors should be careful not to show in tables or figures symmetric error bars that would yield results that are out of range (e.g. negative error rates).
- If error bars are reported in tables or plots, The authors should explain in the text how they were calculated and reference the corresponding figures or tables in the text.

#### 8. Experiments compute resources

Question: For each experiment, does the paper provide sufficient information on the computer resources (type of compute workers, memory, time of execution) needed to reproduce the experiments?

Answer: [Yes]

Justification: All experiments are conducted on one NVIDIA A100 80GB GPU and we provide the time of execution needed to reproduce the experiments. See the Experiments section and Appendix B.7.

#### Guidelines:

- The answer NA means that the paper does not include experiments.
- The paper should indicate the type of compute workers CPU or GPU, internal cluster, or cloud provider, including relevant memory and storage.
- The paper should provide the amount of compute required for each of the individual experimental runs as well as estimate the total compute.
- The paper should disclose whether the full research project required more compute than the experiments reported in the paper (e.g., preliminary or failed experiments that didn't make it into the paper).

#### 9. Code of ethics

Question: Does the research conducted in the paper conform, in every respect, with the NeurIPS Code of Ethics https://neurips.cc/public/EthicsGuidelines?

Answer: [Yes]

Justification: The research conducted in the paper conforms with the NeurIPS Code of Ethics.

#### Guidelines:

- The answer NA means that the authors have not reviewed the NeurIPS Code of Ethics.
- If the authors answer No, they should explain the special circumstances that require a
  deviation from the Code of Ethics.
- The authors should make sure to preserve anonymity (e.g., if there is a special consideration due to laws or regulations in their jurisdiction).

#### 10. Broader impacts

Question: Does the paper discuss both potential positive societal impacts and negative societal impacts of the work performed?

Answer: [Yes]

Justification: The broader impacts of the work are discussed in the Conclusion section.

- The answer NA means that there is no societal impact of the work performed.
- If the authors answer NA or No, they should explain why their work has no societal impact or why the paper does not address societal impact.
- Examples of negative societal impacts include potential malicious or unintended uses (e.g., disinformation, generating fake profiles, surveillance), fairness considerations (e.g., deployment of technologies that could make decisions that unfairly impact specific groups), privacy considerations, and security considerations.
- The conference expects that many papers will be foundational research and not tied to particular applications, let alone deployments. However, if there is a direct path to any negative applications, the authors should point it out. For example, it is legitimate to point out that an improvement in the quality of generative models could be used to generate deepfakes for disinformation. On the other hand, it is not needed to point out that a generic algorithm for optimizing neural networks could enable people to train models that generate Deepfakes faster.
- The authors should consider possible harms that could arise when the technology is being used as intended and functioning correctly, harms that could arise when the technology is being used as intended but gives incorrect results, and harms following from (intentional or unintentional) misuse of the technology.
- If there are negative societal impacts, the authors could also discuss possible mitigation strategies (e.g., gated release of models, providing defenses in addition to attacks, mechanisms for monitoring misuse, mechanisms to monitor how a system learns from feedback over time, improving the efficiency and accessibility of ML).

## 11. Safeguards

Question: Does the paper describe safeguards that have been put in place for responsible release of data or models that have a high risk for misuse (e.g., pretrained language models, image generators, or scraped datasets)?

Answer: [NA]

Justification: The paper poses no such risks.

#### Guidelines:

- The answer NA means that the paper poses no such risks.
- Released models that have a high risk for misuse or dual-use should be released with
  necessary safeguards to allow for controlled use of the model, for example by requiring
  that users adhere to usage guidelines or restrictions to access the model or implementing
  safety filters.
- Datasets that have been scraped from the Internet could pose safety risks. The authors should describe how they avoided releasing unsafe images.
- We recognize that providing effective safeguards is challenging, and many papers do not require this, but we encourage authors to take this into account and make a best faith effort.

## 12. Licenses for existing assets

Question: Are the creators or original owners of assets (e.g., code, data, models), used in the paper, properly credited and are the license and terms of use explicitly mentioned and properly respected?

Answer: [Yes]

Justification: All code, models, and datasets mentioned in the text are appropriately cited with their original papers.

- The answer NA means that the paper does not use existing assets.
- The authors should cite the original paper that produced the code package or dataset.
- The authors should state which version of the asset is used and, if possible, include a URL.
- The name of the license (e.g., CC-BY 4.0) should be included for each asset.

- For scraped data from a particular source (e.g., website), the copyright and terms of service of that source should be provided.
- If assets are released, the license, copyright information, and terms of use in the
  package should be provided. For popular datasets, paperswithcode.com/datasets
  has curated licenses for some datasets. Their licensing guide can help determine the
  license of a dataset.
- For existing datasets that are re-packaged, both the original license and the license of the derived asset (if it has changed) should be provided.
- If this information is not available online, the authors are encouraged to reach out to the asset's creators.

#### 13. New assets

Question: Are new assets introduced in the paper well documented and is the documentation provided alongside the assets?

Answer: [Yes]

Justification: New assets introduced in the paper, such as code, are well documented. The documentation is provided alongside the assets in the supplementary material and anonymous GitHub repository.

#### Guidelines:

- The answer NA means that the paper does not release new assets.
- Researchers should communicate the details of the dataset/code/model as part of their submissions via structured templates. This includes details about training, license, limitations, etc.
- The paper should discuss whether and how consent was obtained from people whose asset is used.
- At submission time, remember to anonymize your assets (if applicable). You can either create an anonymized URL or include an anonymized zip file.

#### 14. Crowdsourcing and research with human subjects

Question: For crowdsourcing experiments and research with human subjects, does the paper include the full text of instructions given to participants and screenshots, if applicable, as well as details about compensation (if any)?

Answer: [NA]

Justification: The paper does not involve crowdsourcing nor research with human subjects. Guidelines:

- The answer NA means that the paper does not involve crowdsourcing nor research with human subjects.
- Including this information in the supplemental material is fine, but if the main contribution of the paper involves human subjects, then as much detail as possible should be included in the main paper.
- According to the NeurIPS Code of Ethics, workers involved in data collection, curation, or other labor should be paid at least the minimum wage in the country of the data collector.

# 15. Institutional review board (IRB) approvals or equivalent for research with human subjects

Question: Does the paper describe potential risks incurred by study participants, whether such risks were disclosed to the subjects, and whether Institutional Review Board (IRB) approvals (or an equivalent approval/review based on the requirements of your country or institution) were obtained?

Answer: [NA]

Justification: The paper does not involve crowdsourcing nor research with human subjects. Guidelines:

 The answer NA means that the paper does not involve crowdsourcing nor research with human subjects.

- Depending on the country in which research is conducted, IRB approval (or equivalent) may be required for any human subjects research. If you obtained IRB approval, you should clearly state this in the paper.
- We recognize that the procedures for this may vary significantly between institutions and locations, and we expect authors to adhere to the NeurIPS Code of Ethics and the guidelines for their institution.
- For initial submissions, do not include any information that would break anonymity (if applicable), such as the institution conducting the review.

#### 16. Declaration of LLM usage

Question: Does the paper describe the usage of LLMs if it is an important, original, or non-standard component of the core methods in this research? Note that if the LLM is used only for writing, editing, or formatting purposes and does not impact the core methodology, scientific rigorousness, or originality of the research, declaration is not required.

Answer: [NA]

Justification: The core method development in this research does not involve LLMs as any important, original, or non-standard components.

- The answer NA means that the core method development in this research does not involve LLMs as any important, original, or non-standard components.
- Please refer to our LLM policy (https://neurips.cc/Conferences/2025/LLM) for what should or should not be described.

## **A Muti-View Information Bottleneck Loss Computation**

As shown in Eq (4), we can wirte the objective of the cell-based hypergraphs  $\mathcal{H}^{C}$  to a loss function as follows:

$$\mathcal{L}^{C} = -\frac{1}{\beta^{C}} I(H^{G}; H_{S}^{C}) + I(H^{C}; H_{S}^{C} \mid H^{G}), \tag{16}$$

where  $\beta^C$  is the trade-off parameter for  $\mathcal{L}^C$ , and we aim to minimize Eq (16) during the training. Similarly, the objective of the grid-based hypergraphs  $H^G$  can be wirtten to a loss function as follows:

$$\mathcal{L}^{G} = -\frac{1}{\beta^{G}} I(H^{C}; H_{S}^{G}) + I(H^{G}; H_{S}^{G} \mid H^{C}), \tag{17}$$

where  $\beta^G$  is the trade-off parameter for  $\mathcal{L}^G$ .

Then, we compute the average loss of  $\mathcal{L}^C$  and  $\mathcal{L}^G$ , which helps us to optimize both  $H_S^C$  and  $H_S^G$ :

$$L_{combination} = \frac{1}{2} \left( -\frac{1}{\beta^C} I(H^G; H_S^C) + I(H^C; H_S^C \mid H^G) \right) + \frac{1}{2} \left( -\frac{1}{\beta^G} I(H^C; H_S^G) + I(H^G; H_S^G \mid H^C) \right)$$

$$= \frac{1}{2} \left( I(H^C; H_S^C \mid H^G) + I(H^G; H_S^G \mid H^C) \right) - \frac{1}{2} \left( \frac{1}{\beta^C} I(H^G; H_S^C) + \frac{1}{\beta^G} I(H^C; H_S^G) \right).$$

For term  $I(H^C; H_S^C \mid H^G)$ , we can derive his upper bound. The conditional mutual information  $I_{\theta}(H^C; H_S^C \mid H^G)$  is defined as:

$$I_{\theta}(H^{C}; H_{S}^{C} \mid H^{G}) = \mathbb{E}_{p(H^{C}, H^{G})} \left[ D_{KL} \left( p_{\theta}(H_{S}^{C} \mid H^{C}) || p_{\theta}(H_{S}^{C} \mid H^{G}) \right) \right], \tag{18}$$

where the Kullback-Leibler (KL) divergence is given by:

$$D_{KL}(p||q) = \mathbb{E}_{p(x)} \left[ \log \frac{p(x)}{q(x)} \right]. \tag{19}$$

Substituting the definition of KL divergence into the conditional mutual information:

$$\begin{split} I_{\theta}(H^C; H_S^C \mid H^G) &= \mathbb{E}_{H^C, H^G \sim p(H^C, H^G)} \mathbb{E}_{H_S \sim p_{\theta}(H_S^C \mid H^C)} \left[ \log \frac{p_{\theta}(H_S^C \mid H^C)}{p_{\theta}(H_S^C \mid H^G)} \right] \\ &= \mathbb{E}_{\mathbf{H}^C, \mathbf{H}^G \sim p(H^C, H^G)} \mathbb{E}_{\mathbf{H}_S \sim p_{\theta}(H_S^C \mid H^C)} \left[ \log \frac{p_{\theta}(H_S^C = \mathbf{H}_S \mid H^C = \mathbf{H}^C)}{p_{\theta}(H_S^C = \mathbf{H}_S \mid H^G = \mathbf{H}^G)} \right]. \end{split}$$

Then, we derive the upper bound of  $I_{\theta}$  ( $H^C; H_S^C \mid H^G$ ):

$$I_{\theta}\left(H^{C}; H_{S}^{C} \mid H^{G}\right) = \mathbb{E}_{\mathbf{H}^{C}, \mathbf{H}^{G} \sim p(H^{C}, H^{G})} \mathbb{E}_{\mathbf{H}_{S} \sim p_{\theta}(H_{S}^{C} \mid H^{C})} \left[ \log \frac{p_{\theta}(H_{S}^{C} = \mathbf{H}_{S} \mid H^{C} = \mathbf{H}^{C})}{p_{\theta}(H_{S}^{C} = \mathbf{H}_{S} \mid H^{G} = \mathbf{H}^{G})} \right]$$

$$= \mathbb{E}_{\mathbf{H}^{C}, \mathbf{H}^{G} \sim p(H^{C}, H^{G})} \mathbb{E}_{\mathbf{H}_{S} \sim p_{\theta}(H_{S}^{C} \mid H^{C})} \left[ \frac{p_{\theta}(H_{S}^{C} = \mathbf{H}_{S} \mid H^{C} = \mathbf{H}^{C})}{p_{\gamma}(H_{S}^{G} = \mathbf{H}_{S} \mid H^{G} = \mathbf{H}^{G})} \cdot \frac{p_{\gamma}(H_{S}^{G} = \mathbf{H}_{S} \mid H^{G} = \mathbf{H}^{G})}{p_{\theta}(H_{S}^{C} = \mathbf{H}_{S} \mid H^{G} = \mathbf{H}^{G})} \right]$$

$$= D_{KL} \left( p_{\theta}(H_{S}^{C} \mid H^{C}) \parallel p_{\gamma}(H_{S}^{G} \mid H^{G}) \right) - D_{KL} \left( p_{\theta}(H_{S}^{C} \mid H^{G}) \parallel p_{\gamma}(H_{S}^{G} \mid H^{G}) \right)$$

$$\leq D_{KL} \left( p_{\theta}(H_{S}^{C} \mid H^{C}) \parallel p_{\gamma}(H_{S}^{G} \mid H^{G}) \right).$$

Similarly, we can get the upper bound for  $I(H^G; H^G_S \mid H^C)$ ):

$$I(H^G; H_S^G \mid H^C)) \le D_{KL} \left( p_{\theta}(H_S^G \mid H^G) \parallel p_{\gamma}(H_S^C \mid H^C) \right).$$

Therefore, the upper bound for the first term is:

$$\frac{1}{2}(I(H^{C}; H_{S}^{C} \mid H^{G}) + I(H^{G}; H_{S}^{G} \mid H^{C}))$$

$$\leq \frac{1}{2}(D_{KL} \left(p_{\theta}(H_{S}^{C} \mid H^{C}) \parallel p_{\gamma}(H_{S}^{G} \mid H^{G})\right) + D_{KL} \left(p_{\theta}(H_{S}^{G} \mid H^{G}) \parallel p_{\gamma}(H_{S}^{C} \mid H^{C})\right))$$

$$= D_{SKL} \left(p_{\theta}(H_{S}^{C} \mid H^{C}) \parallel p_{\gamma}(H_{S}^{G} \mid H^{G})\right),$$

where  $D_{SKL}(\cdot)$  denotes the symmetrized Kullback–Leibler (SKL) divergence.

Then, look at the  $I(H^G; H_S^C)$  in the second term. According to the symmetry of mutual information, i.e., I(X;Y) = I(Y;X), and the chain rule of mutual information, i.e., I(X;Y,Z) = I(X;Y) + I(X;Z|Y), we can have:

$$\begin{split} I(H^G; H_S^C) &= I(H_S^C; H^G) = I(H_S^C; H_S^G, H^G) \\ &= I(H_S^C; H_S^G) + I(H_S^C; H^G | H_S^G). \end{split}$$

Since the conditional mutual information is always non-negative, we can infer:

$$I(H_S^C; H^G | H_S^G) \ge 0.$$
 (20)

Therefore, we can get the lower bound of  $I(H^G; H_S^C)$  as:

$$I(H^G; H_S^C) > I(H_S^C; H_S^G).$$
 (21)

Similarly, for  $I(H^C; H_S^G)$ , we can get,

$$I(H^C; H_S^G) \ge I(H_S^C; H_S^G).$$
 (22)

Therefore, the second term gets the upper bound:

$$\begin{split} & -\frac{1}{2}(\frac{1}{\beta^{C}}I(H^{G};H_{S}^{C}) + \frac{1}{\beta^{G}}I(H^{C};H_{S}^{G})) \\ & \leq -\frac{1}{2}(\frac{1}{\beta^{C}}I(H_{S}^{C};H_{S}^{G}) + \frac{1}{\beta^{G}}I(H_{S}^{C};H_{S}^{G})) \\ & = -\frac{\beta^{C} + \beta^{G}}{2\beta^{C}\beta^{G}}I(H_{S}^{C};H_{S}^{G}). \end{split}$$

Therefore, the combination loss has an upper bound:

$$L_{combination} \leq D_{SKL} \left( p_{\theta}(H_S^C \mid H^C) \parallel p_{\gamma}(H_S^G \mid H^G) \right) - \frac{\beta^C + \beta^G}{2\beta^C \beta^G} I(H_S^C; H_S^G).$$

By scaling both terms with  $\beta = \frac{2\beta^C\beta^G}{\beta^C + \beta^G}$  and re-parameterizing the objective, we derive a tractable loss function for the MVIB framework:

$$\mathcal{L}_{MVIB} = -I(H_S^C; H_S^G) + \beta D_{SKL} \left( p_{\theta}(H_S^C \mid H^C) \parallel p_{\gamma}(H_S^G \mid H^G) \right), \tag{23}$$

where  $p_{\theta}(H_S^C \mid H^C)$  and  $p_{\gamma}(H_S^G \mid H^G)$  represent the bottleneck subgraph extractors for  $H^C$  and  $H^G$  parameterized by  $\theta$  and  $\gamma$  respectively, and  $D_{SKL}(\cdot)$  denotes the symmetrized Kullback–Leibler (SKL) divergence. The hyperparameter  $\beta$  controls the trade-off between the two terms.

## **B** Mathematical Notations

Tables 5 and 6 summarize the mathematical notations used throughout the MIHC framework. Table 5 covers the fundamental problem formulation and basic Information Bottleneck concepts, while Table 6 details the components specific to multi-view representation learning and bottleneck mechanisms. Together, these notations describe the dual hypergraph structures that enable balanced fusion of topological and geometric circuit information for interpretable congestion prediction.

## C Experimental Details

#### C.1 Code Availability.

Our code is available in this link: https://github.com/hping666/MIHC.

Table 5: Mathematical Notations I: Problem Formulation and Information Bottleneck Framework

Notation	Description
$\overline{}$	Number of message passing layers
P	Grid-based layout representation, $\in \mathbb{R}^{M \times N \times K}$
M, N	Grid dimensions
K	Number of features per grid cell
G	Cell-based hypergraph representation, $(V, E)$
V	Set of nodes (cells)
$E_{\underline{}}$	Set of hyperedges (nets)
$C^G$	Grid congestion map, $\in \mathbb{R}^{M \times N}$
$egin{array}{c} C^C \ \hat{C^G} \end{array}$	Cell congestion graph, $\in \mathbb{R}^{ V }$
$\hat{C^G}$	Predicted grid congestion map
$\hat{C^C}$	Predicted cell congestion graph
$f_{ heta}$	Predictive model parameterized by $\theta$
$\mathcal{L}_{ ext{sup}}$	Supervised loss function
$X^{\cdot}$	Input variable in Information Bottleneck framework
Y	Target variable in Information Bottleneck framework
T	Intermediate representation in Information Bottleneck framework
I(T;X)	Mutual information between $T$ and $X$
I(T;Y)	Mutual information between $T$ and $Y$
$\beta^*$	Trade-off parameter in Information Bottleneck framework
$H^C$	Cell-based hypergraph
$H^G$	Grid-based hypergraph
$V^C$	Node set in cell-based hypergraph
$E^C$	Hyperedge set in cell-based hypergraph
$egin{array}{c} X_v^C \ V^G \end{array}$	Feature of node $v$ in cell-based hypergraph
	Node set in grid-based hypergraph
$E^G$	Hyperedge set in grid-based hypergraph
$X_v^G$	Feature of node $v$ in grid-based hypergraph

## **C.2** Hypergraph Construction Details

As shown in Figure 1(a) of our paper, we construct hypergraphs from circuit data through a specific process. In the layout example of Figure 1(a), we have 10 circuit components (cells), each represented as a node in the cell-based hypergraph. The layout is simultaneously divided into 9 grid cells, with each grid cell becoming a node in the grid-based hypergraph. The circuit nets connecting multiple circuit components are modeled as hyperedges in both representations. For the cell-based hypergraph, cells connected by the same net form a hyperedge. As illustrated in Figure 1(c) in the top-left diagram, blue cells 2, 5, 6, and 7 are connected by the same net, thus forming one hyperedge in the cell-based hypergraph.

For the grid-based hypergraph, grid cells traversed by the same net are connected via a hyperedge. Additionally, spatially adjacent grid cells are also connected through hyperedges to preserve geometric proximity information. As shown in Figure 1(c) in the bottom-left diagram, green grid cells 1, 4, 5, and 6 are traversed by the same net, thus forming one hyperedge in the grid-based hypergraph. Simultaneously, adjacent grid cells like 1-2, 2-3, 4-5, etc., would form their own hyperedges based on spatial adjacency.

## C.3 ISPD-2015 Benchmark Dataset

The ISPD-2015 benchmark consists of 20 industrial designs from various applications, with circuit sizes ranging from 29K to 1.3M cells, as shown in Table 7. These designs include both standard cells and macro blocks, presenting realistic challenges in placement and routing congestion prediction. Each design in the dataset includes:

- · Circuit netlist information with both standard cells and macro blocks
- Placement solutions generated using Cadence Innovus v17.1 with varying parameters

Table 6: Mathematical Notations II: Multi-View Representation Learning and Bottleneck Components

Notation	Description
$H_S^C$	Bottleneck subgraph of cell-based hypergraph
$H_S^G \ eta^C$	Bottleneck subgraph of grid-based hypergraph
$eta^C$	Trade-off parameter for cell-based Information Bottleneck
$p_{ heta}, p_{\gamma}$	Probability model for bottleneck subgraph extraction
$\mathbf{M}^C$	Incidence matrix of cell-based hypergraph
$\mathbf{X}^C$	Node features of cell-based hypergraph
$\mathbf{p}_{\underline{}}$	Probability vector for node selection
$\mathbf{X}_{S_{-}}^{C}$	Node features of cell-based bottleneck subgraph
$\mathbf{x}_{S}^{C} \ \mathcal{N}(v^{G}) \ W^{C}, W^{G}$	Cell nodes associated with grid node $v^G$
$W^C, W^G$	Learnable weights for feature reweighting
$\mathcal{L}_{MVIB}$	Multi-View Information Bottleneck loss
$D_{SKL}$	Symmetrized KL divergence
$h_{e}^{C}$	Hyperedge embedding in cell-based hypergraph
$h_e^G$	Hyperedge embedding in grid-based hypergraph
$\mathcal{V}^{\mathcal{C}}(e)$	Nodes in cell-based hyperedge $e$
$\mathcal{V}^{\mathcal{G}}(e)$	Nodes in grid-based hyperedge $e$
$h_e^N$	Net-based hyperedge embedding
$h_{e}^{C}$ $h_{e}^{G}$ $\mathcal{V}^{C}(e)$ $\mathcal{V}^{G}(e)$ $h_{e}^{N}$ $\hat{h}_{v}^{C}$ $\mathcal{E}^{C}(v)$	Intermediate cell-based node embedding
$\hat{h}_v^N$	Intermediate net-based node embedding
$\mathcal{E}^C(v)$	Cell-based hyperedges containing node $v$
$\mathcal{E}^N(v)$	Net-based hyperedges containing node $v$
$\begin{array}{c} \mathcal{E}^{N}(v) \\ h_{v}^{C'} \\ \hat{h}_{v}^{G} \\ \mathcal{N}^{\mathcal{G}}(v) \\ h_{v}^{G'} \\ h_{S}^{C} \\ \mathcal{L}_{\text{cont}} \end{array}$	Updated cell-based node embedding
$\hat{h}_v^G$	Intermediate grid-based node embedding
$\mathcal{N}^{\mathcal{G}}(v)$	Spatially adjacent grid nodes to node $v$
$h_v^{G'}$	Updated grid-based node embedding
$h_S^C$	Cell-based subgraph embedding
$h_S^{\widecheck{G}}$	Grid-based subgraph embedding
$\mathcal{L}_{ ext{cont}}^{B}$	Contrastive loss
au	Temperature parameter in contrastive loss
$\hat{y}_v^C$	Predicted cell-based node congestion
$egin{array}{c}  au \ \hat{y}_v^C \ \hat{y}_v^G \end{array}$	Predicted grid-based node congestion
$\mathcal{L}_{ ext{total}}$	Total loss function

• Ground truth congestion maps derived from global routing solutions

The dataset provides several key features for congestion prediction:

- RUDY (Rectangular Uniform wire DensitY): Models the routing demand within bounding boxes of nets
- PinRUDY: Represents pin density distribution in grid cells
- MacroRegion: Binary indicators for regions covered by macro cells
- Horizontal/Vertical MacroMargin: Measures distances between margins of adjacent macros

For experimentation purposes, 533 different placement solutions were generated for each design using Innovus with varying parameters, resulting in a comprehensive dataset for training and evaluating congestion prediction models. The dataset divides the circuit layout into an  $M \times N$  grid, with each grid cell represented as a pixel containing multiple feature channels. The routing overflow ground truth is provided in both horizontal and vertical directions.

## C.4 CircuitNet-N28 Benchmark Dataset

The CircuitNet-N28 is a comprehensive open-source dataset specifically designed for machine learning applications in VLSI CAD, particularly for cross-stage prediction tasks. It contains 10242

Table 7: Detailed Information of ISPD-2015 Benchmark Designs

Design	#Cells	#Nets	Category
des_perf_1	113K	113K	Medium
des_perf_a	109K	110K	Medium
des_perf_b	113K	113K	Medium
edit_dist_a	130K	131K	Medium
fft_1	35K	33K	Small
fft_2	35K	33K	Small
fft_a	34K	32K	Small
fft_b	34K	32K	Small
matrix_mult_1	160K	159K	Large
matrix_mult_2	160K	159K	Large
matrix_mult_a	154K	154K	Large
matrix_mult_b	151K	152K	Large
matrix_mult_c	151K	152K	Large
pci_bridge32_a	30K	30K	Small
pci_bridge32_b	29K	29K	Small
superblue11_a	954K	936K	Very Large
superblue12	1.3M	1.3M	Very Large
superblue14	634K	620K	Very Large
superblue16_a	698K	697K	Very Large
superblue19	522K	512K	Very Large

layout samples extracted from versatile runs of commercial design tools based on six open-source RISC-V designs in a 28nm technology node, as shown in Table 8.

- Circuit data is generated from six RISC-V designs (RISCY, RISCY-FPU, zero-riscy, and their variants)
- Layouts are generated using commercial tools (Cadence Innovus v20.10) with diverse parameter settings
- Ground truth labels include congestion, DRC violations, and IR drop information

The dataset provides several key features for prediction tasks:

- Macro Region: Regions covered by macros which are fixed during placement
- Cell Density: Cell distribution in each tile
- RUDY & Pin RUDY: Routing demand estimation for nets and pin density
- Pin Configuration: High-resolution representation of pin and routing blockage patterns
- Congestion: Overflow of routing demand in each tile

CircuitNet-N28 introduces significant diversity through various design parameters, including five core utilization settings (70%-90%), three macro placement strategies, eight power mesh combinations, and different filler insertion approaches. This results in 240 combinations of settings for each netlist, creating a dataset with substantial variation that better reflects real-world design scenarios. The tile size for all feature maps is 1.5  $\mu$ m × 1.5  $\mu$ m, aligning with the global routing cell size in commercial tools.

Table 8: Detailed Information of CircuitNet-N28 Benchmark Designs

Design	#Cells	#Nets	Cell Area ( $\mu$ m <sup>2</sup> )
RISCY-a	45,717	47,759	65,739
RISCY-FPU-a	65,793	68,351	75,985
zero-riscy-a	34,299	43,970	58,631
RISCY-b	31,311	33,970	69,979
RISCY-FPU-b	51,126	54,327	80,030
zero-riscy-b	20,946	22,692	62,648

## C.5 Data Split Strategies

We employ two distinct data partitioning strategies to comprehensively evaluate our model's performance and generalization capability: placement-level split and design-level split.

## C.5.1 Placement-level Split

The placement-level split follows a standard design-level partitioning strategy where all designs appear in both training and testing sets, but with different placement solutions. As shown in Table 7, the ISPD2015 dataset contains 20 circuit designs, each with multiple placement solutions generated using different synthesis and placement parameters. For each design, we divide its corresponding placements into training and testing sets with a 7:3 ratio. This results in:

- **ISPD2015-F**: 374 training samples and 159 testing samples (all 20 designs including superblue series, 533 total placements)
- **ISPD2015-B**: 269 training samples and 114 testing samples (15 designs excluding superblue series, 383 total placements)

For CircuitNet-N28 (Table 8), we follow a similar approach across its 10,242 samples from six RISC-V designs, resulting in 7,170 training samples and 3,072 testing samples, maintaining the 7:3 ratio. This approach ensures all designs appear in both training and testing sets, allowing for comprehensive evaluation of model performance on known design types.

## C.5.2 Design-level Split for Generalization Evaluation

To rigorously evaluate our model's generalization capability to entirely unseen circuit designs, we conduct additional experiments following the design-level split setting. Unlike the placement-level split, this setting ensures training and test sets contain completely different circuit designs with no overlap between design families, providing a more stringent evaluation that better reflects real-world scenarios where models must generalize to new designs during deployment.

**ISPD2015-B Design Partitioning** For ISPD2015-B containing 15 designs, we partition them into two groups ensuring designs with the same prefix remain together:

- **Group A** (8 designs): des\_perf\_1, des\_perf\_a, des\_perf\_b, fft\_1, fft\_2, fft\_a, fft\_b, edit\_dist\_a
- **Group B** (7 designs): matrix\_mult\_1, matrix\_mult\_2, matrix\_mult\_a, matrix\_mult\_b, matrix\_mult\_c, pci\_bridge32\_a, pci\_bridge32\_b

**ISPD2015-F Design Partitioning** For ISPD2015-F containing 20 designs, we use a 10 vs 10 split:

- **Group A** (10 designs): des\_perf series (3 designs: des\_perf\_1, des\_perf\_a, des\_perf\_b), fft series (4 designs: fft\_1, fft\_2, fft\_a, fft\_b), edit\_dist\_a, superblue12, superblue16\_a
- **Group B** (10 designs): matrix\_mult series (5 designs: matrix\_mult\_1, matrix\_mult\_2, matrix\_mult\_a, matrix\_mult\_b, matrix\_mult\_c), pci\_bridge32 series (2 designs: pci\_bridge32\_a, pci\_bridge32\_b), superblue11\_a, superblue14, superblue19

This partitioning strategy ensures that:

- 1. Designs with the same prefix (indicating functional similarity) remain in the same group, preventing information leakage between functionally related circuits
- 2. Both groups contain a mix of different design families and sizes
- The evaluation captures the model's true capability to handle entirely unseen circuit architectures

**Bidirectional Evaluation** We conduct bidirectional evaluation to provide comprehensive assessment:

1. **A→B**: Train on all placement solutions from Group A designs, test on all placement solutions from Group B designs

2. **B**→**A**: Train on all placement solutions from Group B designs, test on all placement solutions from Group A designs

This bidirectional approach ensures our evaluation is not biased by the specific choice of training/testing groups and provides robust evidence of generalization performance across different design families.

#### C.6 Evaluation Metrics Details

This study employs a variety of evaluation metrics to assess the performance of the proposed model, including NMAE, NRMS, Pearson correlation, Spearman correlation, Kendall's tau for chip congestion prediction and Accuracy (ACC) for graph anomaly detection. Below are the definitions and mathematical formulations of each metric:

**Normalized Mean Absolute Error (NMAE):** NMAE measures the average absolute difference between predicted and true values, normalized by the range of the true values. It is defined as:

NMAE = 
$$\frac{1}{n} \sum_{i=1}^{n} \frac{|y_i - \hat{y}_i|}{\max(y) - \min(y)}$$
,

where  $y_i$  is the true value,  $\hat{y}_i$  is the predicted value, and  $\max(y)$  and  $\min(y)$  represent the maximum and minimum values of the true data, respectively. A lower NMAE indicates better predictive accuracy.

**Normalized Root Mean Square Error (NRMS):** NRMS quantifies the deviation between the predicted and actual values, normalized by the range of the true values. It is computed as:

NRMS = 
$$\frac{1}{\max(y) - \min(y)} \sqrt{\frac{1}{n} \sum_{i=1}^{n} (y_i - \hat{y}_i)^2}$$
.

This metric penalizes larger errors more heavily, making it useful for evaluating prediction accuracy.

**Pearson Correlation Coefficient (Pearson):** The Pearson correlation coefficient measures the linear relationship between the predicted and true values, with values ranging from -1 (perfect negative correlation) to 1 (perfect positive correlation). It is given by:

$$\text{Pearson} = \frac{\sum_{i=1}^{n} (y_i - \bar{y})(\hat{y}_i - \bar{\hat{y}})}{\sqrt{\sum_{i=1}^{n} (y_i - \bar{y})^2 \sum_{i=1}^{n} (\hat{y}_i - \bar{\hat{y}})^2}},$$

where  $\bar{y}$  and  $\bar{y}$  represent the mean of the true and predicted values, respectively.

**Spearman Rank Correlation (Spearman):** Spearman's rank correlation coefficient assesses the monotonic relationship between the true and predicted values by considering their ranks. It is calculated as:

Spearman = 
$$1 - \frac{6\sum_{i=1}^{n} d_i^2}{n(n^2 - 1)}$$
,

where  $d_i$  is the difference in ranks for each pair of corresponding values, and n is the number of data points.

**Kendall's Tau (Kendall):** Kendall's tau is another measure of rank correlation, specifically focusing on the concordance and discordance between pairs of predictions. It is defined as:

$$\text{Kendall} = \frac{C - D}{\frac{n(n-1)}{2}},$$

where C is the number of concordant pairs, D is the number of discordant pairs, and n is the number of data points.

#### **C.7** Parameter Setting

In this section, we present the key implementation details of our model. The detailed parameter settings are listed in Table 9.

The key parameters include:

Table 9: Model Parameter Settings

Parameter	Value	Parameter	Value
Hidden Dimension	128	Learning Rate	1e-4
# MV-HGNN Layers	4	Batch Size	4
# MLP Layers	2	Temperature $\tau$	0.07
IB Weight $\beta$	0.1	Dropout Rate	0.1
# Attention Heads	4	Optimizer	Adam

- Hidden Dimension: The dimension of node embeddings in both cell-based and grid-based views.
- # MV-HGNN Layers: Number of Multi-View Heterogeneous Graph Neural Network layers.
- # MLP Layers: Number of layers in the prediction module MLPs.
- **IB Weight**  $\beta$ : The trade-off parameter in Information Bottleneck loss.
- **Temperature**  $\tau$ : Temperature parameter in contrastive learning.
- # Attention Heads: Number of attention heads in message passing.

The model is trained using the Adam optimizer with a learning rate of 1e-4. We apply dropout with rate 0.1 to prevent overfitting. The batch size is set to 32 for training efficiency.

#### C.8 Time Consumption and Memory Usage

#### **C.8.1** Time Consumption

Our experiments on one NVIDIA A100 80GB GPU show practical performance across circuit scales. Small circuits (30K cells/nets) require only 0.3 seconds for inference and 0.9 seconds per training iteration, while very large circuits (1.3M cells/nets) take 1.6 seconds for inference and 5.0 seconds per training iteration. These measurements confirm that despite the model's sophistication, its computational demands remain manageable for real-world industrial applications, with reasonable inference times even for the largest circuits.

#### C.8.2 Memory Usage

Our model's memory footprint scales efficiently with circuit size. Small circuits (30K cells/nets) consume approximately 3GB of GPU memory, while even the largest circuits (1.3M cells/nets) require 22GB during training, well within the 80GB capacity of modern A100 GPUs, ensuring our approach remains practical for industrial-scale designs.

## D Result Supplement

## **D.1** Chip Congestion Prediction Results

Table 10: Cell based Results on ISPD2015-B. The best in **bold** and the second <u>underlined</u>.

Model	ISPD2015-B								
Model	NMAE↓	NRMS↓	Pearson <sup>↑</sup>	Spearman†	Kendall <sup>↑</sup>				
GCN	0.038	0.044	0.547	0.498	0.421				
GAT	0.039 (-2.63%)	0.045 (-2.27%)	0.531 (-2.94%)	0.517 (+3.81%)	0.463 (+9.95%)				
HGNN	0.036 (+5.26%)	0.042 (+4.55%)	0.577 (+5.50%)	0.553 (+11.05%)	0.476 (+13.07%)				
CircuitGNN	0.034 (+10.53%)	0.040 (+9.09%)	0.598 (+9.33%)	0.611 (+22.68%)	0.487 (+15.68%)				
LHNN	0.033 (+13.16%)	0.038 (+13.64%)	0.629 (+14.99%)	0.627 (+25.90%)	0.502 (+19.24%)				
DE-HNN	0.032 (+15.79%)	0.037 (+15.91%)	0.645 (+18.00%)	0.632 (+26.91%)	0.520 (+23.56%)				
MIHC(Ours)	0.029 (+23.68%)	0.034 (+22.73%)	0.687 (+25.66%)	0.689 (+38.43%)	0.574 (+36.38%)				

Table 11: Grid based Results on ISPD2015-B and ISPD2015-F. The best in **bold** and the second underlined.

Model			ISPD2015-B		
Model	NMAE↓	NRMS↓	Pearson <sup>↑</sup>	Spearman↑	Kendall↑
GCN	0.043	0.049	0.405	0.162	0.137
GAT	0.044 (-2.33%)	0.050 (-2.04%)	0.398 (-1.73%)	0.144 (-11.12%)	0.141 (+2.92%)
HGNN	0.040 (+6.98%)	0.046 (+6.12%)	0.451 (+11.36%)	0.184 (+13.58%)	0.142 (+3.65%)
RouteNet	0.038 (+11.63%)	0.045 (+8.16%)	0.522 (+28.89%)	0.198 (+22.22%)	0.157 (+14.60%)
CircuitGNN	0.037 (+13.95%)	0.043 (+12.24%)	0.561 (+38.39%)	0.201 (+24.07%)	0.164 (+19.71%)
CircuitFormer	0.034 (+20.93%)	0.040 (+18.37%)	0.649 (+60.74%)	0.231 (+42.59%)	0.169 (+23.36%)
LHNN	0.033 (+23.26%)	0.040 (+18.37%)	0.651 (+60.74%)	0.252 (+55.56%)	0.217 (+58.39%)
Lay-Net	0.031 (+27.91%)	0.037 (+24.49%)	0.667 (+64.57%)	0.301 (+85.19%)	0.248 (+81.76%)
MIHC (Ours)	0.030 (+30.23%)	$\overline{0.036} (+26.53\%)$	0.675 (+66.67%)	0.297 (+83.95%)	0.252 (+83.94%)

Table 12: Cell based Results on ISPD2015-F. The best in **bold** and the second <u>underlined</u>.

Model			ISPD2015-F		
Model	NMAE↓	NRMS↓	Pearson↑	Spearman↑	Kendall↑
GCN	0.051	0.058	0.344	0.336	0.309
GAT	0.050 (+1.96%)	0.057 (+1.72%)	0.351 (+2.03%)	0.342 (+1.79%)	0.298 (-3.55%)
HGNN	0.045 (+11.76%)	0.052 (+10.34%)	0.410 (+19.21%)	0.366 (+8.93%)	0.309 (0.00%)
CircuitGNN	0.046 (+9.80%)	0.053 (+8.62%)	0.402 (+16.85%)	0.378 (+12.50%)	0.316 (+2.27%)
LHNN	0.043 (+15.69%)	0.049 (+15.52%)	0.448 (+30.23%)	0.384 (+14.29%)	0.364 (+17.80%)
DE-HNN	0.042 (+17.65%)	0.048 (+17.24%)	0.467 (+35.80%)	0.395 (+17.57%)	0.381 (+23.32%)
MIHC(Ours)	0.035 (+31.37%)	0.041 (+29.31%)	0.524 (+52.33%)	0.512 (+52.38%)	0.447 (+44.64%)

Table 13: Grid based Results on ISPD2015-F. The best in **bold** and the second underlined.

Model			ISPD2015-F								
	NMAE↓	NRMS↓	Pearson <sup>†</sup>	Spearman↑	Kendall↑						
GCN	0.046	0.053	0.357	0.152	0.131						
GAT	0.048 (+4.35%)	0.055 (+3.77%)	0.331 (-7.28%)	0.137 (-9.87%)	0.116 (-11.47%)						
HGNN	0.043 (+6.52%)	0.050 (+5.66%)	0.352 (-1.40%)	0.147 (-3.29%)	0.121 (-7.63%)						
RouteNet	0.042 (+8.70%)	0.050 (+5.66%)	0.362 (+1.40%)	0.161 (+5.92%)	0.137 (+4.58%)						
CircuitGNN	0.042 (+8.70%)	0.049 (+7.55%)	0.364 (+2.00%)	0.162 (+6.58%)	0.134 (+2.29%)						
CircuitFormer	0.038 (+17.39%)	0.045 (+15.09%)	0.453 (+26.91%)	0.196 (+28.95%)	0.165 (+26.02%)						
LHNN	0.037 (+19.57%)	0.044 (+16.98%)	0.464 (+29.97%)	0.221 (+45.39%)	0.182 (+38.93%)						
Lay-Net	0.035 (+23.91%)	0.042 (+20.75%)	0.484 (+35.53%)	0.256 (+68.42%)	0.208 (+58.02%)						
MIHC (Ours)	0.032 (+30.43%)	0.039 (+26.42%)	0.503 (+41.00%)	0.271 (+78.95%)	$\overline{0.227 (+73.25\%)}$						

Table 14: Cell based Results on CircuitNet-N28. The best in **bold** and the second underlined.

Model	CircuitNet-N28								
Model	NMAE↓	NRMS↓	Pearson <sup>†</sup>	Spearman↑	Kendall↑				
GCN	0.045	0.051	0.516	0.438	0.319				
GAT	0.046 (-2.22%)	0.051 (+0.00%)	0.513 (-0.58%)	0.447 (+2.05%)	0.321 (+0.63%)				
HGNN	0.044 (+2.22%)	0.048 (+5.88%)	0.552 (+6.98%)	0.468 (+6.85%)	0.332 (+4.08%)				
CircuitGNN	0.040 (+11.11%)	0.043 (+15.69%)	0.609 (+18.02%)	0.500 (+14.16%)	0.368 (+15.36%)				
LHNN	0.039 (+13.33%)	0.043 (+15.69%)	0.617 (+19.57%)	0.509 (+16.21%)	0.366 (+14.73%)				
DE-HNN	0.038 (+15.56%)	0.042 (+17.65%)	0.638 (+23.64%)	0.511 (+16.67%)	0.374 (+17.24%)				
MIHC(Ours)	0.036 (+20.00%)	0.039 (+23.53%)	0.661 (+28.10%)	0.522 (+19.18%)	0.396 (+24.14%)				

## **D.2** Expalination Results

Due to the lack of publicly available, interpretable datasets in the EDA domain, we use the commonly adopted MNIST 0/1 dataset to demonstrate the explainability of our proposed MIHC. To validate the effectiveness of the explainability module in our model, we conduct explainability testing experiments on these datasets to test our model's capability in identifying important nodes in the graph through node-level explainability testing. The results of these tests are presented in Table 16. Our proposed method demonstrates strong consistency across both datasets, exhibiting high performance across various evaluation metrics. This suggests that our approach provides reliable and coherent explanations across different types of data, indicating that the model's interpretability is robust and can generalize well. The consistent high scores in all the key metrics underscore the model's ability to

Table 15: Grid based Results on CircuitNet-N28. The best in **bold** and the second <u>underlined</u>.

Model			CircuitNet-N28			
Model	NMAE↓	NRMS↓	Pearson↑	Spearman↑	Kendall↑	
GCN	0.052	0.053	0.417	0.399	0.312	
GAT	0.052 (+0.00%)	0.054 (-1.89%)	0.411 (-1.44%)	0.405 (+1.50%)	0.323 (+3.53%)	
HGNN	0.051 (+1.92%)	0.052 (+1.89%)	0.442 (+6.00%)	0.424 (+6.27%)	0.331 (+6.09%)	
RouteNet	0.047 (+9.62%)	0.049 (+7.55%)	0.541 (+29.74%)	0.501 (+25.56%)	0.373 (+19.55%)	
CircuitGNN	0.047 (+9.62%)	0.048 (+9.43%)	0.547 (+31.18%)	0.508 (+27.32%)	0.371 (+18.91%)	
CircuitFormer	0.044 (+15.38%)	0.046 (+13.21%)	0.622 (+49.16%)	0.526 (+31.83%)	0.384 (+23.08%)	
LHNN	0.043 (+17.31%)	0.044 (+16.98%)	0.646 (+54.92%)	0.533 (+33.58%)	0.389 (+24.68%)	
Lay-Net	0.041 (+21.15%)	0.043 (+18.87%)	0.671 (+60.91%)	0.558 (+39.85%)	0.406 (+30.13%)	
MIHC (Ours)	0.040 (+23.08%)	$\overline{0.041}$ (+22.64%)	0.682 (+63.55%)	0.572 (+43.36%)	0.402 (+28.85%)	

Table 16: Node explanation test on MNIST0 and MNIST1. The best in **bold** and the second underlined.

Dataset	Method	ACC	Precision	Recall	F1	AUC
	ours	0.742	0.669	0.725	0.696	0.697
$\mathbf{S}\mathbf{I}$	GCN+GNNE	0.527	0.343	0.500	0.407	0.554
MNIST0	GAT+GNNE	0.419	0.349	0.917	0.506	0.689
	SIGNET	0.650	0.995	0.041	0.078	0.615
MNIST1	ours	0.721	0.642	0.698	0.669	0.685
	GCN+GNNE	0.527	0.359	0.583	0.444	0.573
	GAT+GNNE	0.419	0.321	0.708	0.442	0.594
	SIGNET	<u>0.650</u>	1.000	0.041	0.079	0.522

offer actionable and meaningful insights for decision-making in practical applications. In comparison, baseline methods show significant limitations. GAT+GNNE suffers from low precision despite high recall, while SIGNET achieves high precision but fails to capture comprehensive node relationships, leading to low recall scores. The core principle of explainability—identifying the most important part of the graph—remains the same across both MNIST and chip congestion scenarios.

Furthermore, to demonstrate MIHC's explainability under realistic congestion scenarios, we present a chip congestion heatmap in Figure 2. This visualization highlights the model's capability to accurately localize critical regions on the chip. As clearly shown, MIHC achieves the closest match to the ground truth, underscoring its superior interpretability.

#### **D.3** Hyper-parameter Sensitivity

Detailed results of hyper-parameter sensitivity are shown in Table 17 and Table 18.

Table 17: Hidden Dimension Sensitivity Analysis on ISPD2015-B

Tuble 17. Theden Dimension Sensitivity That years on 191 D 2019 B										
Hidden Dim		C	ell-based R	esults		Grid-based Results				
	NMAE↓	NRMS↓	Pearson↑	Spearman <sup>†</sup>	Kendall↑	NMAE↓	NRMS↓	Pearson↑	Spearman↑	Kendall↑
32	0.036	0.040	0.579	0.592	0.484	0.041	0.045	0.477	0.199	0.151
64	0.030	0.036	0.663	0.668	0.551	0.032	0.037	0.662	0.281	0.246
128	0.029	0.034	0.687	0.689	0.574	0.030	0.036	0.675	0.297	0.252
256	0.029	0.034	0.682	0.688	0.577	0.030	0.036	0.676	0.294	0.250

Table 18: Multi-view HGNN Layer Number Sensitivity Analysis on ISPD2015-B

								<i>'</i>		
#Layers	Cell-based Results						Gı	rid-based R	esults	
πLayers	NMAE↓	NRMS↓	Pearson <sup>↑</sup>	Spearman†	Kendall↑	NMAE↓	NRMS↓	Pearson <sup>†</sup>	Spearman†	Kendall↑
1	0.033	0.039	0.612	0.619	0.492	0.039	0.044	0.510	0.192	0.148
2	0.030	0.035	0.679	0.672	0.566	0.031	0.036	0.672	0.290	0.251
3	0.029	0.034	0.690	0.681	0.571	0.030	0.036	0.672	0.294	0.252
4	0.029	0.034	0.687	0.689	0.574	0.030	0.036	0.675	0.297	0.252
5	0.030	0.034	0.688	0.684	0.571	0.030	0.037	0.671	0.288	0.247
6	0.030	0.035	0.671	0.666	0.554	0.031	0.037	0.669	0.288	0.248